HHS Public Access

Author manuscript

Exp Neurol. Author manuscript; available in PMC 2019 May 01.

Published in final edited form as:

Exp Neurol. 2018 May ; 303: 12–28. doi:10.1016/j.expneurol.2018.01.005.

NEURONAL *PTEN* DELETION IN ADULT CORTICAL NEURONS TRIGGERS PROGRESSIVE GROWTH OF CELL BODIES, DENDRITES, AND AXONS

Erin A. Gallent[1,2,5] and **Oswald Steward**[1,2,3,4,5]

[1]Reeve-Irvine Research Center, University of California, Irvine

[2]Department of Anatomy and Neurobiology, University of California, Irvine

[3]Department of Neurobiology and Behavior, University of California, Irvine

[4]Department of Neurosurgery, University of California, Irvine

[5]School of Medicine, University of California, Irvine

Abstract

Deletion of the phosphatase and tensin (*PTEN*) gene in neonatal mice leads to enlargement of the cell bodies of cortical motoneurons (CMNs) in adulthood (Gutilla et al., 2016). Here, we assessed whether *PTEN* deletion in adult mice would trigger growth of mature neurons. *PTEN* was deleted by injecting AAV-Cre into the sensorimotor cortex of adult transgenic mice with a lox-P flanked exon 5 of the *PTEN* gene and Cre-dependent reporter gene tdTomato. PTEN-deleted CMN's identified by tdT expression and retrograde labeling with fluorogold (FG) were significantly enlarged four months following *PTEN* deletion, and continued to increase in size through the latest time intervals examined (12–15 months post-deletion). Sholl analyses of tdT-positive pyramidal neurons revealed increases in dendritic branches at 6 months following adult *PTEN* deletion, and greater increases at 12 months. 12 months after adult *PTEN* deletion, axons in the medullary pyramids were significantly larger and G-ratios were higher. Mice with PTEN deletion exhibited no overt neurological symptoms and no seizures. Assessment of motor function on the Rotorod and cylinder test revealed slight impairment of coordination with unilateral deletion; however, mice with bilateral *PTEN* deletion in the motor cortex performed better than controls on the rotarod at 8 and 10 months post-deletion. Our findings demonstrate that robust neuronal growth can be induced in fully mature cortical neurons long after the developmental period has ended and that this continuous growth occurs without obvious functional impairments.

Corresponding Author: Oswald Steward, Ph.D., Reeve-Irvine Research Center, 837 Health Sciences Dr., University of California Irvine School of Medicine, Irvine, CA 92697, osteward@uci.edu.

Conflict of Interest: OS is one of the co-founders of the company "Axonis", which holds options on patents relating to PTEN deletion and axon regeneration.

Keywords

Aging; motor cortex; cortical pyramidal neurons; *PTEN*; mTOR; animal

INTRODUCTION

Neurons in the adult central nervous system have a low intrinsic ability to regenerate, accounting for limited recovery following trauma, damage due to stroke, or neurodegenerative processes. Experimental attempts to increase the regenerative potential of injured adult axons have identified the phosphatase and tensin gene (*PTEN*) as an important negative regulator of axon regeneration. In optic nerve crush and spinal cord injury models, injured axons that originate from *PTEN* deleted neurons exhibit robust regeneration (Liu et al., 2010; Park et al., 2008). In these studies, AAV-Cre was injected into the eye or spinal cord of *PTEN* floxed mice to delete *PTEN* in retinal ganglion cells in the optic nerve crush injury, or neurons of the motor cortex in the spinal cord injury model respectively. Subsequent studies revealed regenerative growth of corticospinal (CST) axons following *PTEN* deletion in mature mice and after AAV-shRNA-mediated knockdown in mature rats, which was accompanied by recovery of motor function (Danilov and Steward, 2015; Du et al., 2015; Lewandowski and Steward, 2014; Zukor et al., 2013).

The above studies highlight the potential of therapeutic applications targeting *PTEN* to enhance regeneration; however, the long-term consequences of interventions targeting *PTEN* in a therapeutically-relevant way (in adult animals) are unknown. *PTEN* is a phosphatase that catalyzes the conversion of PIP3 to PIP2, countering the action of phosphatidylinositol-3-kinase (PI3K). Accordingly, *PTEN* deletion leads to increases in PIP3, resulting in increased activation of Akt and mammalian target of rapamycin (mTOR). mTOR is an important regulator of neuronal growth, including axon growth and guidance and dendritic outgrowth (Jaworski and Sheng, 2006).

Several studies have assessed the consequences of *PTEN* deletion during embryonic or early postnatal development. For example, promoter-driven deletion of *PTEN* in neurons expressing neuron specific enolase (NSE) or Ca^{2+}/calmodulin-dependent protein kinase II (CAMKII) leads to striking neuronal hypertrophy and macrocephaly. Physiological studies reveal impaired long-term potentiation (LTP) and spontaneous seizures have been detected by electroencephalography (EEG) (Kwon et al., 2006; Sperow et al., 2012; Takeuchi et al., 2013). Knockdown of *PTEN* in postnatally derived dentate granule cells via injection of short hairpin RNA or injections of retroviruses expressing Cre recombinase into *PTEN*ff mice leads to increased excitatory drive of dentate granule cells, and increases in total dendrites, dendritic spines, and synapses (Luikart et al., 2011; Williams et al., 2015).

We recently assessed the long-term consequences of deleting *PTEN* in the sensorimotor cortex at postnatal day 1, using the approach that enables regeneration of CST axons following spinal cord injury in adults (Gutilla et al., 2016; Liu et al., 2010). Following unilateral AAV-Cre injections into the sensorimotor cortex of *PTEN* floxed mice at P1, we found substantial hypertrophy of cortical motoneuron cell bodies in mice that had survived for 1 year. We did not assess different time points after AAV-Cre injection so an unresolved

question is whether this cellular growth occurs only during development or continues throughout life. Of even greater interest is whether *PTEN* deletion in mature neurons would initiate a new phase of cellular growth after neurons have ceased growing in adulthood.

The goals of the present study were to determine whether *PTEN* deletion in adult cortical motoneurons also triggered neuronal growth and if so, whether growth was transient or continuous. To address these questions, we used double transgenic mice in which Cre-mediated recombination deletes *PTEN* and activates expression of tdTomato in the same neurons. We show that *PTEN* deletion via intracortical injection of AAV-Cre leads to progressive enlargement of cortical neuronal cell bodies that continues for over 1 year, increases in dendritic arborization as revealed by Sholl analysis, and increases in axonal diameter. Analyses of motor function at different times post *PTEN* deletion revealed no difference in motor function in comparison to controls at early time points but enhanced motor function in the oldest mice.

METHODS

PTEN deletion in the motor cortex of adult mice

The Institutional Animal Care and Use Committee (IACUC) at the University of California, Irvine approved all experimental procedures. Doubly transgenic mice were generated by breeding mice with lox-P flanked exon 5 of the *PTEN* gene (RRID: IMSR_JAX:004597) to mice with a lox-P flanked STOP cassette in the ROSA locus that prevents expression of tandem dimer tomato (tdTomato) fluorescent protein (RRID: IMSR_JAC:007905). We will refer to these mice as PTEN/tdT mice for brevity. Transgenic control mice harbor only the lox-P flanked STOP cassette within the ROSA locus that prevents tdTomato expression (referred to hereafter as tdT mice). Table 1 summarizes the number of mice used for each assessment.

Surgical procedures

For all surgical procedures, mice were anesthetized with Isoflurane (2–3%), their eyes were swabbed with Vaseline, and the skin at the incision site was shaved and cleaned with Betadine. Following completion of the surgery, mice were returned to their home cages on 37°C water circulating heating pads until they recovered from the anesthetic.

To delete *PTEN* in adult cortical neurons, PTEN/tdT mice (n=26) received unilateral intracortical injections of AAV-Cre recombinase at 8 or more weeks of age. Transfection by AAV-Cre results in the excision of exon 5 of the *PTEN* gene and the STOP cassette for tdTomato, resulting in deletion of *PTEN* and expression of tdTomato in the same neurons. To control for any effect due to AAV injections, tdT control mice received identical unilateral injections of AAV-Cre. The vectors were AAV serotype 2, and were obtained from Vector Bio Labs (1×10^{13} genome copies/mL, Catalog number 7011). The vector was diluted with sterile-filtered PBS and 5% glycerol for a final concentration of 1×10^{12} genome copies/mL.

For intracranial injections, a midline scalp incision was made. Burr holes were placed in the skull overlying the cortical areas to be injected and 4 unilateral intracortical injections of

AAV-Cre were made into the sensorimotor cortex using a Hamilton syringe with a pulled glass micropipette (1.0mm lateral and 0.5mm depth at +0.5mm, −0.2mm, −0.5mm, and −1.0mm relative to bregma). Each injection was 0.6µl in volume, for a total injection volume of 2.4µl. Injections were performed over one minute and the microsyringe was left in place for three minutes.

Retrograde labeling of cortical motoneurons

To definitively identify the cells of origin of corticospinal tract axons (cortical motoneurons), PTEN/tdT (n= 26) and tdT mice (n=10) mice received bilateral intraspinal injections of the retrograde tracer Fluorogold 3, 4, 5, 6, 7, 9, 12, and 15 months following AAV-Cre injections. Mice were prepared for surgery as above, and a C5 laminectomy was performed to expose the spinal cord. Two injections of 0.2µl of 1% Fluorogold were made with a Hamilton syringe with a pulled glass micropipette at 0.5mm lateral to the midline at 0.5mm depth. Fluorogold was injected over one minute and the syringe was left in place for an additional minute. After completing the injections, the muscles were sutured with 5.0 chromic gut and the skin was closed with staples. Mice received subcutaneous injections of buprenorphine, Baytril and lactated Ringer's twice a day for three days post-operatively and were kept in their home cages for 3–4 days prior to tissue collection.

Tissue collection and histology

3–4 days after receiving Fluorogold injections, mice received intraperitoneal injections of Fatal-Plus (1mL/300g) and were transcardially perfused with 4% paraformaldehyde (PFA). Brains and spinal cords were dissected and allowed to postfix for 48 hours in 4% PFA before being placed overnight in 30% sucrose/phosphate buffered saline (PBS) for cryoprotection. For Vibratome sectioning, tissue blocks were attached to blocks with cyanoacrylate and sectioned at 200µm or 40µm. Sections were collected in serial order in wells containing PBS with 0.1% NaN3. Tissue sectioned on the cryostat was embedded in OCT compound (Tissue-Tek) and frozen by immersion in a container with methyl butane surrounded by crushed dry ice/ethanol slurry. Brains were sectioned in the coronal plane at 20µm and collected in wells with PBS with 0.1% NaN3.

To visualize neurons co-labeled with tdTomato and Fluorogold, tdTomato fluorescence was visualized directly without immunostaining. To visualize Fluorogold, 20–40µm sections were incubated overnight at room temperature with rabbit anti-Fluorogold (RRID: AB_2314407) diluted to 1:600 in 5% NDS, 5% BSA, 0.4% triton-X in 50mM KPBS. Sections were then incubated with an anti-rabbit biotinylated secondary antibody (1:250, RRID: AB_2313606), followed by incubation in avidin and biotinylated horseradish peroxidase (1:100, RRID: AB_2336819), and FITC labeling (made in house, 1:250 dilution in 0.001%H202 borate buffer). Stained sections were slide mounted and cover slipped with Vectashield mounting medium (RRID: AB_2336789).

Sections (one every 200µm) were stained for H&E or cresyl violet, and/or immunostained for different markers (below). For immunostains other than Fluorogold, an antigen retrieval protocol was used in which sections were placed in 1.7ml Eppendorf tubes with 1mL 10mM citrate buffer, pH 8.80. Tubes were then immersed in boiling water for 5 minutes, placed on

ice for 5 minutes, and left at room temperature for 10 minutes. Primary antibodies and dilutions were as follows: PTEN (1:250, AB_390810), two phospho-specific antibodies for ribosomal protein S6 (1:250 for both, Ser 235/236: RRID: AB_916156, Ser 240/244: RRID: AB_331682), and glial fibrillary acid protein (GFAP, 1:2000, RRID: AB_100013482). PTEN and pS6 antibodies were diluted in Blocking Reagent (PerkinElmer), all other antibodies were diluted in 5% secondary antibody host serum in TBS or PBS with 0.3% Triton (GFAP).

Sections were incubated in primary antibody overnight at room temperature, and then in secondary antibodies in the same blocking solution for two hours at room temperature. For immunofluorescence, we used Alexa Fluor 488 (RRID: AB_2535792) or Alexa Fluor 594 (RRID: AB_141637), both at 1:250 dilution. For sections undergoing DAB detection, sections were incubated in a biotinylated IgG secondary antibody (1:250, RRID: AB_2313606), washed 3 times, incubated for 1 hour with avidin and biotinylated horseradish peroxidase (1:100, RRID: AB_2336819) and reacted with DAB (RRID: AB_2336382).

Cortical motoneuron cell size measurements

To measure the cell body size of CMNs over time following *PTEN* deletion in adulthood, we used the data from a previously conducted pilot experiment in a power/sample size calculation to determine the minimum number of mice that could be used for each time point. Each time point used for cell body size measurements had a minimum of 3 PTEN/tdT mice (3 months: n=4, 2 females, 2 males, 4 months: n=3, 0 females, 3 males, 5 months: n=4, 2 females, 2 males, 6 months: n=3, 3 females, 0 males, 7 months: n=3, 0 females, 3 males, 9 months: n= 3, 0 females, 3 males, 12 months: n= 3, 0 females, 3 males, 15 months: n=3, 3 females, 0 males). Two tdT control mice were used for cell size measurement at 3, 6, 9, 12, and 15 month time points (3 month: 2 females, 0 males, 6 months: 1 female, 1 male, 9 months: 0 females, 2 males, 12 months: 1 female, 1 male, 15 months: 2 females, 0 males). For the mid-life *PTEN* deletion analyses, 3 PTEN/tdT mice (1 female, 2 males) were assessed at 2 months post-deletion and 5 PTEN/tdT mice (2 females, 2 males) were assessed at 5 months post-deletion. A random number generator was used to determine surgical order and to assign mice to groups.

Cortical motoneurons (CMNs) were identified by retrograde labeling with Fluorogold and *PTEN* deleted neurons were identified by their expression of tdTomato. Neurons co-labeled by both Fluorogold and tdTomato must therefore be *PTEN* deleted CMNs. For cell size measurements, sections that were immunostained for Fluorogold were imaged by 2-photon microscopy for both Fluorogold and tdTomato. The cortical region containing the highest density of neurons co-labeled with tdTomato and Fluorogold was identified, and image stacks were collected (1024 by 1024μm, depth of 20–40μm, step distance 0.5μm). Image stacks of the same size were collected from the homotopic region of the contralateral cortex containing CMNs labeled with FG only. Image stacks were reconstructed in 3D and 2-dimensional projections were generated from the 3D image stacks, and analyzed in ImageJ.

We measured the cross-sectional area of 50 *PTEN* deleted, Fluorogold positive CMNs in the area of deletion. Sampling was done by measuring all colabeled cells starting at the lateral

aspect of the motor cortex and moving medially, until 50 colabeled cells had been measured. As an intra-animal control, we then measured 50 Fluorogold positive (*PTEN* intact) CMNs in the homotopic cortical region on the contralateral side of the same section using the same lateral-medial sampling strategy. To control for possible effects of transfection by AAV-Cre and tdTomato expression on cell size, we performed identical analyses in tdT mice with intact *PTEN* expression, measuring 50 tdTomato/Fluorogold positive CMNs vs. 50 Fluorogold positive CMNs on the contralateral side. All measurements were done blind to mouse genotype, however the large effect of *PTEN* deletion on cell size made it difficult for the person conducting the analysis to remain blind.

The average values per mouse were then averaged across mice in the time point, in order to calculate the overall mean cross-sectional area for the *PTEN* deletion and control groups at each time point with n=number of mice. Measures of cell body size were analyzed using repeated measures two-way analysis of variance (ANOVA), and comparisons of cell size between time points were done using Sidak's multiple comparisons post-hoc analysis. Since there were no significant differences between the intra-animal controls and the AAV injection control mice, statistics are reported using only the intra-animal controls.

Characterization of dendritic arbor

To assess the dendritic arbor of pyramidal neurons following adult *PTEN* deletion, mice that had received AAV-Cre injections only were euthanized 6 months (n= 6 PTEN/tdT mice, 4 tdT mice) and 12 months (n= 7 PTEN/tdT mice, 6 tdT mice) post-deletion. These time points were chosen because of the continuing growth of CMN cell bodies we observed from 6–12 months. Mice received injections of Fatal Plus as above, were perfused transcardially with 4% PFA, and brains were post-fixed for 48 hours in 4% PFA. The unfrozen brains were adhered to a block with cyanoacrylate and sectioned on a Vibratome into 200μm sections that were collected in PBS with 0.1% NaN3.

Sections used for 3D imaging were cleared using a passive CLARITY protocol. On day 1, sections were incubated in 4% acrylamide PBS with 0.25% VA-044 thermal initiator at 4°C for 48 hours. The sections were then transferred to a 37°C oven to allow the acrylamide to polymerize. Once polymerized, the sections were washed in PBS for 30 minutes to 1 hour at room temperature and then were placed in 25mM borate 500mM sodium dodecyl sulfate (SDS) overnight at 37°C. The following day, sections were transferred to fresh borate SDS solution and left at 37°C overnight, and this was repeated on the next day. After three nights in borate SDS solution, the sections were washed 4 times in PBS over an 8-hour span at room temperature and were then submerged in Sorbitol F overnight at room temperature. Sections were then mounted and cover slipped with Sorbitol F for imaging.

3D Imaging and Sholl Analysis

Cleared, thick sections were imaged in 3D using a 3i video-rate two-photon laser scanning microscope on the Olympus BX51WIF platform (Olympus America Inc., Center Valley, PA) equipped with a Chameleon Ti:sapphire laser (Coherent, Santa Clara, CA). The laser beam is focused through a 20X water-immersion objective (numerical aperture 0.95) and emitted fluorescence is detected by photomultipliers (Hamamatsu, Middlesex, NJ) to derive a video

signal that is captured and analyzed using SlideBook 6.0 (Intelligent Imaging Innovations, Inc., Santa Monica, CA).

tdTomato labeled neurons were selected for imaging based on the following criteria: 1) Neuron had pyramid-shaped soma; 2) Neuron was located near the middle of the section, and not close to a section edge, to avoid asymmetric truncation of dendrites; 3) Neuron was isolated in the field of view, or surrounded by only a few other labeled neurons, such that individual dendritic processes could be unequivocally attributed to the correct neuron. Image stacks were collected (1024 by 1024μm, scan depth of 150–200μm, step distance 1.0 μm), and reconstructed in 3D. Stacks were collapsed into 2D images and the dendritic arbor of individual neurons was manually traced.

Traced projections were imported into FIJI, converted to 8-bit binary images, and analyzed using the Sholl Analysis program (Ferreira et al., 2014). Using the center of the soma, concentric circles with an increasing diameter of 10μm were placed on each traced projection, and the number of intersections at each circle was counted. The cross-sectional area of neurons used for Sholl analysis was measured by manually tracing the cell body of the flattened 2D projection in FIJI. The diameter of the apical dendrite was measured 30 μm away from the center of the soma in the flattened 2D projection.

For Sholl analysis data, neurons were analyzed based on time post-AAV injection, either 6 or 12 months (Table 2). For the 6 month time point, 6 PTEN/tdT mice (3 females, 3 males) and 4 tdT mice (3 females, 1 male) were used. For the 12 month time point 7 PTEN/tdT mice (4 females, 3 males) and 6 tdT mice (4 females, 2 males) were used. Table 2 summarizes the number of cells that were analyzed from each mouse. The raw intersection data was analyzed using repeated measures two-way ANOVA, and post-hoc comparisons were done using Sidak's multiple comparisons post-test.

Measurement of axon size in the medullary pyramids

To assess the effect of *PTEN* deletion on the size of uninjured corticospinal (CST) tract axons, we examined CST axons in the medullary pyramids. PTEN/tdT (n= 3) and tdT mice (n=2) mice that had received unilateral AAV-Cre injections were perfused with 2% glutaraldehyde 2% paraformaldehyde. Brains and spinal cords were dissected and allowed to post-fix for 48 hours in 2% glutaraldehyde 2% paraformaldehyde. Tissue was then sunk in 30% sucrose PBS overnight before being cut into thick 200μm sections on a Vibratome. Brainstem sections containing the medullary brainstem were collected and immunostained for tdTomato using an antigen retrieval protocol wherein sections were submerged in centrifuge tubes with ~1 mL 10 mm citrate buffer (pH 8.5–9) and placed in a boiling water bath for 5 minutes. The tubes were then placed on ice for 5 minutes and left to sit at room temperature for 10 minutes. Sections were then incubated with anti-red fluorescent protein (anti-RFP) primary antibody (1:200, RRID: AB_2209751) diluted in 5% NDS and 0.4% Triton in TBS overnight at room temperature. Sections were then incubated with a horseradish peroxidase conjugated secondary antibody (1:250, RRID: AB_2340590) diluted in the same solution as the primary and were then reacted with DAB (RRID: AB_2336382). Following immunostaining, sections were trimmed to isolate the medullary pyramids, stained with Toluidine blue, and processed for electron microscopy (EM).

Sections were scanned at the EM level at low magnification to identify all tdT-labeled axons, and images were taken (185μm^2) of all labeled axons. Images collected by EM were overlaid with a 4μm grid and analyzed in ImageJ. All tdTomato positive axons were measured (26 axons in 1 female and 18 and 25 axons in 2 male PTEN/tdT mice; 16 and 31 axons in two female tdT mice), along with neighboring unlabeled axons in the field that were intersected by a grid crosshair. The cross-sectional area of the axoplasm, axoplasm plus myelin, and myelin alone were measured. G-ratio was calculated as the ratio of the diameter of the axoplasm/the diameter of the axoplasm plus myelin. Data were compared across groups using repeated measures two-way ANOVA, and Sidak's post-test. Differences in G-ratio were analyzed using student's t-test.

Functional testing following unilateral PTEN deletion

For functional testing, we first tested mice that had received unilateral injections of AAV-Cre at 8 weeks of age (PTEN/tdT; n=18 and tdT; n=16). The unilateral injection model allowed separate assessment of limbs controlled by the cortex in which *PTEN* had been deleted vs. the contralateral cortex with intact PTEN expression. At 6 months post-*PTEN* deletion, motor function was tested using a rotarod and cylinder task.

Rotarod testing was done in a way that allowed assessment of motor learning and performance ability (Rothwell et al., 2014). Overall testing consisted of three trials a day over 4 consecutive days, for a total of 12 trials. All testing was done at night based on performance by age-matched controls in pilot studies. The first two days of testing involved slower rotation speeds and were thus less challenging than the third and fourth days. Briefly, on days 1 and 2 the mice were placed on the rod with an initial speed of 4 RPM with an acceleration of 0.1 RPM/s. On days 3 and 4 the initial speed was increased to 6 RPM with an acceleration of 0.2 RPM/s. Each trial was a maximum of 5 minutes and ended if a mouse fell off of the rod. Latency to fall was recorded and the maximum attained speed was calculated for each trial.

Performance on the rotarod was compared by taking the latency to fall for each mouse and calculating the speed at which the mouse fell off the rod (latency to fall * acceleration + starting speed) and averaging this value for each trial based on group (control vs. *PTEN* deletion). The average speed for each trial was then compared between groups using two-way ANOVA. Baseline coordination and motor learning were calculated using linear regression analysis (Rothwell et al., 2014).

The same mice were assessed using the cylinder task. Testing for each task was done on non-consecutive days to avoid fatigue. The cylinder task quantifies the preference of forelimb use during spontaneous exploration and was done once at 6 months following unilateral AAV-Cre injection. The cylinder task was conducted in a completely dark room lit by a red lamp. A 1000mL beaker was placed on a flat surface with the mouth of the beaker open to the environment. A small amount of bedding from the home cage was placed at the bottom of the beaker. A single mouse was then placed in the beaker and videotaped from above for analysis. Forepaw sidedness was recorded each time the mouse reared up and placed one or both forepaws on the walls of the beaker to support body weight. Touches were recorded as R (right forepaw, controlled by the left motor cortex with *PTEN* deletion,

L (left forepaw, controlled by the right motor cortex and no *PTEN* deletion), or B (both forepaws simultaneously). A total of 10 weight-bearing touches were recorded per mouse with the requirement that the mouse had to place both forepaws on the bottom of the beaker between successful paw touches. The recorded percentage of forepaw touches executed by each forepaw (or both) was then used to determine forelimb use asymmetry.

Performance in the cylinder task was measured by taking the raw count of forepaw touch sidedness (out of ten total touches), and comparing forepaw touches between groups (control vs. *PTEN* deletion) by repeated measures two-way ANOVA. Sidak's post-test was used to identify asymmetry in forepaw usage (right forepaw vs. left forepaw vs. both forepaws).

Assessment of motor function over time following bilateral PTEN deletion

Based on our behavioral findings following unilateral *PTEN* deletion in neonatal mice (Gutilla et al., 2016) and the bimanual nature of the rotarod task, we assessed performance on the rotarod and in the cylinder task following bilateral *PTEN* deletion in the motor cortex. 10 PTEN/tdT mice and 9 age-matched tdT control mice received bilateral intracortical injections of AAV-Cre at 8 weeks of age as above (total injection volume of 2.4μl/side).

PTEN/tdT and tdT mice that received bilateral AAV-Cre injections were assessed for motor learning on the rotarod at 2, 4, 6, and 8 months following bilateral AAV-Cre injection as described for mice following unilateral *PTEN* deletion. The same person carried out the testing for each session and was blind to the genotype of the mice. At 8 months following AAV-Cre injection, interim statistical analyses were performed to determine whether to continue behavioral testing. Based on rotarod performance trends from 2–8 months following injection, we assessed rotarod performance at 10 months following injection in order to evaluate the stability of our observed trend.

The same mice were assessed using the cylinder task at 2, 4, 6, and 8 months following *PTEN* deletion as described for mice following unilateral *PTEN* deletion. Testing for each task was on non-consecutive days to avoid fatigue and was conducted by the same person each time who was blind to genotype. Interim statistical analyses at 8 months following AAV-Cre injection did not reveal a trend, so mice were not tested in the cylinder task at 10 months.

RESULTS

AAV-Cre transfection deletes PTEN and induces concurrent tdTomato expression

To achieve *PTEN* deletion in the motor cortex of adult mice, 8-week-old PTEN/tdT mice and 8 week old tdT control mice received identical intracortical injections of AAV-Cre into the left motor cortex. The region of AAV-Cre injection was readily identifiable as a focal region containing tdTomato-expressing cells and processes (Fig. 1A). In both *PTEN* deleted and control cases at all time points, tdTomato labeling extended through all cortical layers.

In our previous study of mice with early postnatal deletion of *PTEN* (Gutilla et al., 2016), we observed hypertrophy of the affected area of the cortex and sometimes there was displacement of the superior sagittal fissue due to cortical enlargement on the side of the

PTEN deletion. In the present study, we also observed focal enlargement of the motor cortex at the site of AAV-Cre injection (a focal cortical bump, see Fig. 1A), but did not observe displacement of the superior sagittal fissue. “Cortical bumps” were seen in both PTEN/tdT and tdT control mice, so the focal cortical enlargement may be due to decompression of the brain at the cranial defect produced by burr holes drilled for intracranial injections.

At the center of the injection region (where tdTomato expression was maximal), there was dense labeling of cell bodies and neuropil by tdTomato creating a fluorescent sphere roughly 1mm in diameter (Fig. 1A). Within this sphere it was difficult to identify individual neurons and their respective processes, however neurons located at the periphery of the core region were identifiable (Fig. 1B). Occasionally we also observed tdTomato-positive neurons in the homotopic region of the contralateral motor cortex (not shown). This is likely due to retrograde transport of AAV-Cre by commissural neurons.

Immunostaining sections for PTEN from PTEN/tdT mice revealed focal deletion of PTEN in the area of tdTomato expression (Fig. 1C). Within the area of deletion, the overall level of immunostaining was reduced; (compare the left and right cortices of Fig. 1B, which illustrates immunostaining in the homotypic region on the contralateral side). Large cells that were completely negative for PTEN appeared as “ghost cells” (Fig. 1D&F). Ghost cells were not evident in the motor cortex contralateral to the region of *PTEN* deletion or in the area of the AAV-Cre injection in tdT mice (Fig. C&E). High magnification views of PTEN immunostained sections using phase contrast microscopy confirmed that ghost cells are in fact large PTEN negative neurons (Fig. 1F&G).

No evident pathology due to PTEN deletion in adulthood

In H&E-stained sections, there was no evident pathology in the area of *PTEN* deletion except for the minor injury produced by the needle track of the Hamilton syringe, which could be seen in some cases. The area of the injection was identifiable by the “cortical bump” and by differences in cytoarchitecture, including less well-defined lamination and decreased cell packing density (Fig. 2A). Even in H&E stains from PTEN/tdT mice, enlarged neuronal cell bodies were evident in the area of deletion (Fig. 2B; Fig. 2C illustrates the homologous region in the contralateral cortex).

In addition to tdTomato-labeled neurons, there were a few tdTomato expressing cells with astrocyte morphology in sections from both PTEN/tdT and tdT mice (Fig. 1B). Sections containing the injection site from PTEN/tdT and tdT mice that were immunostained for glial fibrillary acid protein (GFAP) revealed scattered tdTomato positive, GFAP positive cells around the core of the injection (Fig. 2E), confirming that some astrocytes had been transfected by AAV-Cre. There were no abnormal collections of GFAP positive cells, except at the core of the injection region along the boundary of the needle track created by the penetration of the micropipette attached to the Hamilton syringe (Fig. 2D).

Adult PTEN deletion leads to persistent activation of growth-associated signaling pathways

Early postnatal deletion of *PTEN* in the sensorimotor cortex of mice results in persistent activation of phosphorylation of ribosomal protein S6 in *PTEN*-negative cortical

motoneurons (Gutilla et al., 2016). S6 phosphorylation is considered to be a biomarker for mTOR activation and can be documented by immunostaining for pS6 using phospho-specific antibodies. Immunostaining sections in the area of *PTEN* deletion using pS6 specific antibodies revealed elevated S6 phosphorylation in the area of *PTEN* deletion. The area of *PTEN* deletion (Fig. 2F, left cortex) is clearly delineated by a distinct border between neurons with high levels of pS6 immunostaining vs. neurons exhibiting immunostaining comparable to neurons on the contralateral side (Fig. 2F, right cortex). Neurons in all cortical layers exhibited higher levels of immunostaing, but layer V pyramidal neurons exhibited the highest levels of pS6 in both the cell bodies and proximal dendrites (Fig. 2G). Levels of immunostaining for pS6 remained high at all time points. Indeed, at 15 months following AAV-Cre injection, increased pS6 immunostaining was qualitatively comparable to what is seen 3 months after *PTEN* deletion (Fig. 2F). Increases in immunostaining for pS6 were not seen in control mice that received comparable injections of AAV-GFP (data not shown).

Progressive enlargement of PTEN deleted cortical motoneurons

To assess CMN cell bodies following adult *PTEN* deletion, CMNs were definitively identified by labeling with the retrograde tracer Fluorogold (FG) following bilateral intra-spinal injections of FG at cervical level 5 (C5) and the cell body measurements were done based on colabeling by both markers. Sections from FG-injected mice were immunostained for FG to achieve more complete labeling of cell bodies and dendrites. Figure 3A illustrates a section in which the area of *PTEN* deletion is marked by tdTomato expression and CMNs are retrogradely-labeled with FG.

Sections were imaged by 2-photon microscopy and *PTEN*-negative CMNs identified by co-labeling with both FG and tdTomato (Fig. 3B&D) were compared with FG-positive CMNs in the homotopic region of the cortex contralateral to the AAV-Cre injection (Fig. 3C). 3D image stacks were flattened into 2D projections, and imported into ImageJ and the cross-sectional area of CMNs was manually traced. Identical analyses were done in tdT mice as a control for transfection with AAV-Cre and tdT expression.

Figure 3E–G illustrates the cross-sectional areas of 50 control and 50 *PTEN* deleted CMNs in 3 individual mice at 15 months post-AAV-Cre injection. The average size of *PTEN* deleted and control neurons was calculated for each individual mouse and then the mean across mice was calculated so for statistics, n=number of mice. Figure 3H illustrates the mean cross-sectional area of *PTEN* deleted CMNs in comparison to contralateral control CMNs at different times post-AAV-Cre. Two-way ANOVA revealed an overall difference between groups ($F(1, 37)=107.3$, $p<0.0001$), a significant difference across time ($F(7,37)=4.911$, $p=0.0005$), and a significant interaction ($F(7,37)=3.821$, $p=0.0032$). Sidak's multiple comparisons post-test revealed that there was no significant difference between *PTEN*-negative and control CMNs 3 months following AAV-Cre injection ($p>0.9999$, $t=0.3252$). At all time points 4 or more months following AAV-Cre injection, *PTEN*-negative CMNs were larger than the contralateral control CMNs (see legend of Figure 3 for values). The magnitude of the difference in cross-sectional area between *PTEN* deleted and control CMNs remained consistent from 4 to 9 months following *PTEN* deletion, but cell

size increased further between 12 and 15 months. At 15 months, average CMN cross-sectional area was 310.1 $\mu m^2 \pm 52.40 \mu m^2$ for *PTEN* deleted CMNs vs. 195.8$\mu m^2 \pm 1$ 4.14μm^2 for *PTEN* intact contralateral control CMNs, representing a size difference of 1.6X.

The cross-sectional area of FG-positive CMNs in the contralateral cortex did not differ significantly over time following AAV-injection (Fig. 3I, two-way ANOVA, Sidak's post-test $p>0.9999$ for all time points). For full statistics, see figure legend. Also, there was no significant difference in cross-sectional area between the tdT control CMNs and the intra-animal control CMNs in the cortex contralateral to the AAV-Cre injection.

PTEN deletion in mid-life also results in significant growth of cortical motoneurons

The AAV-Cre injections for the above analyses were done at 8 weeks of age, when the mice are young adults. To determine whether *PTEN* deletion-induced neuronal growth is limited to young adults, we performed identical analyses on PTEN/tdT mice that received AAV-Cre injections at 9 months of age. As illustrated in Figure 3J, there was no significant difference in cross-sectional area 2 months following AAV-Cre injection, but by 5 months *PTEN* deleted CMNs were significantly enlarged (two-way ANOVA, $F(1, 6)= 21.36$ $p=0.0036$ for *PTEN* deletion, $F(1, 6)=1.536$, $p= 0.2615$ for time, $F(1, 6)=2.002$, $p= 0.2069$ for interaction). Post-hoc analysis revealed that differences were significant at 5 months (two-way ANOVA Sidak's post-test, $p=0.0184$) but not at 2 months (two-way ANOVA Sidak's post-test, $p=0.4088$).

Although our analysis of soma size focused on CMNs in layer V, PTEN-deleted neurons in all cortical layers appeared to be enlarged (Figure 1F). Thus, growth induced by PTEN deletion is not restricted to particular neuron types.

Deletion of PTEN in adult cortical pyramidal neurons results in increased dendritic arborization

The Akt-mTOR pathway plays a role in regulating dendritic size and structure (Kumar et al., 2005), and previous studies have documented increases in dendritic size and arborization with *PTEN* deletion in early development (Kwon et al., 2006; Williams et al., 2015). Accordingly, we assessed whether growth of cell bodies was accompanied by dendritic growth by comparing dendritic arbors of *PTEN* deleted tdTomato positive neurons vs. control neurons expressing tdTomato from tdT mice with intact *PTEN* expression.

For the analysis of dendritic arbors, tdTomato positive pyramidal neurons were imaged in 3D using 2-photon microscopy 6 and 12 months following AAV-Cre injections when mice were 8 and 14 months old. For technical reasons, 3D reconstructions were done on pyramidal neurons in layers II/III rather than CMNs. Although the mice had received FG injections into the spinal cord, FG fluorescence was not consistently discernable by 2-photon microscopy without immunostaining, and immunostaining for FG abrogated tdTomato fluorescence in dendrites. Second, tdT labeling in dendrites extending from layer V neurons faded over the imaging interval. For unknown reasons, this was less of a problem for layer II/III pyramidal neurons. Since our goal was to determine whether PTEN deletion in adult neurons triggered growth, the question can be addressed just as well with layer II/III pyramidal neurons as with CMNs. The criteria for inclusion were: 1) pyramid-shaped cell

body; 2) location near the center of the section; 3) isolation from other neurons in the field of view to allow accurate identification of dendrites belonging to the selected neuron.

The area containing selected tdT-labeled pyramidal neurons was imaged by 2-photon microscopy, collecting image stacks 1024 by 1024μm, scan depth of 150–200μm, step distance 1μm. Image blocks of this size capture dendritic branches out to approximately 300μm in the plane of the thick section, which is oriented along the long axis of the neuron and out to approximately 75–100μm perpendicular to the plane of the thick section (half the distance of the section thickness). The image stacks were reconstructed in 3D using Imaris. For Sholl analysis, image stacks were collapsed into a 2D projection image, imported into ImageJ and dendrites were traced manually and analyzed using the Sholl Analysis program (Ferreira et al., 2014).

At the 6 month time point, we analyzed the dendritic arbor of 13 pyramidal neurons from 6 PTEN/tdT mice and 11 cells from 4 tdT mice. Figure 4A&B illustrate examples of collapsed 3D images of neurons from control tdT and PTEN/tdT mice respectively. Tracings of these neurons with concentric circles overlaid are illustrated in Figure 4C&E respectively along with heat maps generated by the Sholl analysis program (Fig. 4D&F); warmer colors indicate the distances away from the soma at which the maximal number of dendritic intersections occurred and cooler colors indicate the distances at which the fewest dendrites intersected the concentric circles. The graph in Figure 4G plots the average number of intersections at different distances from the soma in control vs. *PTEN* deleted neurons. The total number of intersections summed across distances was significantly higher for *PTEN* deleted neurons by ANOVA (*PTEN* deleted vs. control: $F(1,590)=65.05$, $p<0.0001$, distance: $F(26,590)=69.56$, $p<0.0001$, interaction: $F(26,590)=1.73$, $p= 0.0145$). To assess whether increased branching occurred at a particular distances from the soma, we compared the number of intersections at different distances from the soma by Bonferroni's multiple correction test; this revealed significant differences in intersections at distances from 90–130μm from the soma (for statistics see figure legend).

At 12 months following *PTEN* deletion, we analyzed 44 cells from 7 PTEN/tdT mice and 23 cells from 6 tdT mice. Figure 5A&B illustrate examples of collapsed 3D images of neurons from control tdT mice and PTEN/tdT mice respectively, along with tracings of these neurons with heat maps in Figure 5C–F. Figure 5G plots the average number of intersections at different distances from the soma in control vs. *PTEN* deleted neurons. The total number of intersections summed across distances was significantly higher for *PTEN* deleted neurons compared to tdT control neurons (*PTEN* deleted vs. controls: $F(1, 1735)= 552.7$ $p< 0.0001$, for distance $F(26, 1735)= 172.4$ $p< 0.0001$, for interaction $F(26, 1735)= 17.02$ $p< 0.0001$). Comparisons of number of intersections at different distances from the soma by Bonferroni's multiple correction test revealed that differences in the number intersections were significant across a wider range of distances from the soma compared to 6 months. ($p< 0.05$ for 40μm to 160μm at 12 months compared to 90μm to 130μm for 6 months, see Figure legend for statistics).

To assess the progression of changes in dendritic parameters in *PTEN*-deleted neurons, we compared data sets at 6 and 12 months post-AAV injection. Comparisons of Sholl data from

PTEN deleted neurons revealed overall increased dendritic branches at 12 month vs. 6 months post-deletion (Fig. 6A, F(1, 1153)= 4.484 p= 0.0344) and overall significant differences across distance (F(26, 1153)= 71.94 p< 0.0001) with no significant interaction F(26, 1153)= 0.9145 p= 0.5886). Posthoc comparisons by Bonferroni's multiple correction test revealed no significant differences at partcular distances away from the soma, however.

We also quantified other parameters: 1) the cross-sectional area of the soma and diameter of the apical dendrite and the ratio between these; 2) the number of primary dendrites emanating from the cell body (separated into the apical and basal dendrites depending on their point of origin from the soma); 3) the total number of dendritic branch points for each neuron.

For the analysis of cell body size and subsequent analyses, we used two way ANOVA with *PTEN* status and time post-deletion. Confirming the findings with FG-labeled CMNs, the cell bodies of *PTEN*-deleted layer II/III neurons were significantly larger than controls (Figure 4H and 5H respectively; two-way ANOVA: F(1, 87)=114.1 p< 0.0001), and there were significant differences between the time points F(1, 87)=17.80, p< 0.0001). Post hoc comparisons by Sidak's test revealed that cell body size of *PTEN*-deleted neurons was significantly larger at 12 vs. 6 months post-deletion (t=3.72, p=0.0014).

Apical dendritic diameter was also larger for *PTEN*-deleted layer II/III neurons vs. control neurons (Fig. 4I and Fig. 5I; two-way ANOVA: (F(1, 87)=99.24 p< 0.0001, Sidak's multiple comparisons post-test for 6 month *PTEN* deletion vs. controls t=4.470 p<0.0001, for 12 months *PTEN* deletion vs. controls t=11.61 p<0.0001) and there were significant differences between the time points F(1, 87)=15.20, p< 0.0002). Post-hoc comprisons using the Holm-Sidak method revealed that increases in apical dendrite diameter were greater at 12 vs. 6 months (t=4.006, p<0.0002). The ratio of dendritic diameter to cross-sectional area of the soma was significantly greater in *PTEN*-deleted vs. controls (Fig. 4J and Fig. 5J, F(1, 87)=13.12, p< 0.0001) but there were no significant differences between time points (F(1, 87)=0.82, p=0.367). Sidak's post-test revealed no significant difference in the ratio between *PTEN* deleted neurons and controls at 6 months (t=1.123 p=0.8419), however *PTEN* deleted neurons had significantly greater ratio values compared to control neurons at 12 months (t=5.023 p<0.0001).

Overall, *PTEN* deleted neurons at both time points had more primary dendrites emanating from the soma than control neurons (Fig. 4K and 5K, two-way ANOVA, for *PTEN* status F(1, 87)= 18.36, p<0.0001). There was no significant difference between the two time points or significant interaction between time and *PTEN* status (for time F(1, 87)= 0.2328 p=0.6306, for interaction F(1,87)=0.9716 p=0.3270). Differences in total number of primary dendrites were not significant at 6 months (Sidak's post-test, t=1.948 p=0.2860) but were significant at 12 months (t=4.955, p<0.0001). At 12 months, the increase in total number of primary dendrites in *PTEN* deleted neurons was due a larger number of primary basal dendrites compared to controls (Fig. 5K: Sidak's post-test, for basal dendrites t=3.416 p=0.0058), with no significant differences in the number of apical dendrites (t=2.433 p=0.0978). Differences between *PTEN* deleted neurons at 6 vs. 12 months and control neurons at 6 vs. 12 months were not significant for total primary dendrites, basal primary

dendrites, or apical primary dendrites (Fig. 6C and 6G, Sidak's post-test for *PTEN* deletion total primary dendrites 6 vs. 12 months t=0.3855 p=0.9993, *PTEN* deletion basal primary dendrites 6 vs. 12 months t=0.8116, p=0.9616, *PTEN* deletion apical primary dendrites 6 vs. 12 months t=0.4980 p=0.9970, control total primary dendrites 6 vs. 12 months t=0.9688 p=0.9138, control basal primary dendrites 6 vs. 12 months t=0.5168 p=0.9963, control apical primary dendrites 6 vs. 12 months t=1.837 p=0.3512).

The maximal number of intersections indicates the maximal number of dendritic segments intersecting concentric circles at any distance from the cell body. Overall, *PTEN* deleted pyramidal neurons had a larger maximal number of intersections than controls, and post-hoc analyses revealed that differences in intersections were significant at 12 months but not 6 (Fig. 4L and 5L, for *PTEN* status $F(1, 87)= 27.43$ $p<0.0001$, for time $F(1,87)=0.1695$ $p=0.6816$, for interaction $F(1,87)= 7.908$ $p=0.0061$, Sidak's post-test comparing *PTEN* deletion and controls at 6 months $t=1.423$ $p=0.6380$, for 12 months $t=7.567$ $p<0.0001$). Comparisons of the values from *PTEN* deleted pyramidal neurons at 6 vs. 12 months revealed no significant differences (Fig. 6C, $t=2.470$ $p=0.0892$). Differences between control neurons at 6 and 12 months were also not significant (Fig. 6G, $t=1.584$ $p=0.5256$).

PTEN deleted layer II/III pyramidal neurons also had more dendritic branch points than controls (Fig. 4M and 5M, two-way ANOVA, for *PTEN* status $F(1, 87)= 29.71$ $p<0.0001$, for time $F(1, 87)= 2.952$ $p=0.0893$, for interaction $F(1,87)=1.716$ $p=0.1937$). For *PTEN* deleted pyramidal neurons, the number of dendritic branch points was significantly increased compared to controls at 12 but not 6 months (Fig. 4M and 5M, Sidak's post-test, for *PTEN* deletion vs. controls at 6 months $t=2.445$ $p=0.0950$, for 12 months $t=6.356$ $p<0.0001$). Differences in number of branch points between *PTEN* deleted neurons at 6 and 12 months were not significant (Fig. 6D, $t=0.3129$ $p=0.9998$), and there was no significant effect of time overall ($F(1, 87)= 2.952$, $p=0.0893$). Post-hoc comparisons revealed that while the number of dendritic branch points of control neurons decreased between 6 and 12 months, the differences were not significant (Fig. 6H, $t=1.998$, $p=0.2595$).

Control pyramidal neurons with intact PTEN expression exhibit age-related dendritic loss

Comparison of dendritic intersections in *PTEN* deleted pyramidal neurons at 6 and 12 months psot-deletion revealed a significant increase in intersections with time (Fig. 6A, for time post-deletion $F(1,1153)=4.484$ $p=0.0344$, for distance from soma $F(26,1153)=71.94$ $p<0.0001$, for interaction $F(26, 1153)=0.9145$ $p=0.5886$). To assess the stability of dendritic parameters in control neurons, we compared data sets at 6 and 12 months post-AAV injection. Comparisons of Sholl data (Fig. 6E) revealed that the number of dendritic intersections in Sholl analysis was significantly decreased at 12 vs. 6 months for control neurons (time following injection $F(1, 582)= 6.215$ $p= 0.0129$, distance $F(23, 582)= 33.83$ $p< 0.0001$, interaction $F(23, 582)=0.5312$ $p=0.9654$). Posthoc comparisons by Bonferroni's multiple correction test revealed no significant differences at partcular distances away from the soma, however.

Analysis of other dendritic parameters of control neurons at 12 vs. 6 months revealed no significant differences in the total number of primary dendrites (Fig. 6F, $t=1.708$, $p=0.097$), the number of basal dendrites ($t=0.529$, $p=0.6003$). Despite a trend towards fewer maximal

intersections and branch points at 12 vs. 6 months, these differences were not significant (Fig. 6G and 6H, Sidak's post-test, maximal intersections t=1.584 p=0.5256, branch points t=1.998 p=0.2595).

PTEN deletion leads to enlargement of corticospinal tract axons without altering myelination

To examine the effect of adult *PTEN* deletion on axon size and myelination, we identified *PTEN* deleted axons in the medullary pyramids of three PTEN/tdT mice by tdT immunostaining and compared these to neighboring un-labeled control axons. The same analysis was done for tdT-positive axons in the medullary pyramid of two tdT mice. Brainstem sections were immunostained for tdTomato using DAB. One micron sections were stained with Toluidine blue, and ultrathin sections were processed for electron microscopy. tdT-positive (*PTEN* deleted) axons were easily identified at the electron microscopic level (Fig. 7A&E). These and neighboring tdT-negative control axons were manually traced, and axoplasm cross-sectional area, axoplasm plus myelin cross-sectional area, myelin cross-sectional area, axoplasm diameter, and axoplasm plus myelin diameter were measured. The ratio of the diameter of the axoplasm and the diameter of the axoplasm plus myelin was used to calculate the G-ratio.

Two-way ANOVA revealed significant differences based on *PTEN* status (Fig. 7B,: ($F(1, 12)= 15.35$ $p= 0.0020$), and structure measured ($F(2, 12)= 11.66$ $p= 0.0015$), witn no significant interaction ($F(2, 12)= 2.481$ $p= 0.1254$). Cross-sectional areas of tdT-labeled axons were significantly larger in PTEN/tdT mice (Fig. 7B, Sidak's post-test $p= 0.0373$). The cross-sectional areas of tdT-positive axons in tdT control mice were very similar to the unlabeled controls in both genotypes (Fig. 7B&F). There were no significant differences in cross-sectional area of myelin alone (Fig. 7C, Sidak's post-test $p= 0.9577$), but there were significant differences in the values for axoplasm plus myelin area (Sidak's post-test $p= 0.0159$).

G-ratios were significantly higher for *PTEN*-deleted axons compared to controls (Fig. 7D, students t-test=87.01, p=0.0005, df=4). Taken together, the unchanged cross-sectional area of myelin and the increased G-ratio seen in *PTEN* deleted axons one year following adult deletion indicate that *PTEN* deletion-induced increase in axon diameter does not trigger compensatory increases in myelination. Cross-sectional areas of myelin on tdT-labeled axons in tdT mice (*PTEN* intact) did not differ significantly from neighboring controls in any of the measurements (Figure 7F–H, see figure legend for statistics). Also, the cross-sectional areas of myelin on tdT-positive axons in tdT control mice were very similar to that of unlabeled axons in both genotypes (Fig. 7B&F).

Unilateral adult PTEN deletion impairs motor coordination but does not affect symmetry of forelimb use during exploration

To examine the functional effects of unilateral *PTEN* deletion in the adult motor cortex, mice were tested on the rotarod and cylinder task. Testing was done 6 months after unilateral AAV-Cre injection in 8-week-old PTEN/tdT mice (n=18) and age-matched tdT mice with intact *PTEN* expression (n=16). The rotarod task has been used to assess both motor

performance and motor learning (Rothwell et al., 2014). With repeated trials, mice exhibit an improved ability to remain on the accelerating rotating rod. Improvement in performance over time is considered a measure of motor learning, peak performance is considered a measure of motor performance ability, and initial performance is a measure of baseline coordination.

We assessed mice on the rotarod across 4 consecutive days with 3 trials/day (12 total trials). Trials 1–6 on days 1 and 2 of testing entailed less challenging test parameters (slower starting speed, slower acceleration), and trials 7–12 on days 3 and 4 were more challenging (faster starting speed, faster acceleration). This design was utilized to prevent masking of continued performance improvements by a ceiling effect that is typically observed in the absence of a challenge. Latency to fall was measured and used to calculate maximum attained speed for each trial.

Both groups exhibited improved rotarod performance across trials 1–7 (increased latency to fall and higher average maximum speed attained with each successive trial) (Fig. 8A). On trials 8–12, both groups exhibited a plateau in performance. Two-way ANOVA revealed that both *PTEN* deletion status and trial number had a significant effect on maximum terminal speed attained ($F(1, 636)= 38.06$ $p<0.0001$ for *PTEN* status; $F(11, 3378)= 18.38$ $p<0.0001$ for trial number, $F(11, 25)= 0.1359$ $p= 0.9996$ for interaction**,** though the differences at individual trials were not significant.

To determine whether baseline deficits in motor coordination or impaired motor learning was responsible for the reduced performance of mice with unilateral adult *PTEN* deletion, we analyzed the data by linear regression (Rothwell et al., 2014). The slope of the line calculated from maximum terminal speed over successive trials, interpreted as motor learning (dashed lines), did not differ significantly between the two groups (0.7384 ± 0.1058 RPM/trial for controls and 0.7917 ± 0.199 RPM/trial for *PTEN* deletion, student's t-test $p=0.7304$, $F(1, 20)=0.1221$) (Fig. 8A). The calculated y-intercept, interpreted as baseline motor coordination (horizontal dashed lines), was significantly lower for mice with *PTEN* deletion compared to controls (7.263 ± 0.7787 RPM for controls and 4.415 ± 0.8089 RPM for *PTEN* deletion, student's t-test $F(1, 21)=23.5419$, $p<0.0001$).

Since the rotarod data were obtained using two paradigms of the same task, we also performed segmental linear regression analysis, analyzing trials 1–6 (pre-challenge) and 7–12 (challenge) separately. The y-intercept (baseline coordination) for controls was 5.689 and 1.173 RPM for *PTEN* deletion cases, again indicating that unilateral adult *PTEN* deletion impairs baseline coordination. The pre-challenge rate of learning (slope) for trials 1–6 was 1.202 RPM/trial for controls and 1.173 RPM/trial for *PTEN* deletion cases, representing a slight impairment in motor learning during the easier trials. Following the challenge of increased starting speed and increased acceleration in trials 7–12, the rate of learning for controls was 0.3781 RPM/trial and 0.4958 RPM/trial for mice with *PTEN* deletion. Taken together the data suggest that the *PTEN* deletion group has slightly impaired motor learning under easier circumstances, and improved learning level under challenging circumstances. Ultimately, the *PTEN* deletion group failed to achieve a maximum terminal speed equal to

that of the control group (15.0375 RPM in trial 9 for controls and 12.844 RPM in trial 7 for *PTEN* deletion).

The same mice were also tested in the cylinder task to determine if unilateral *PTEN* deletion during adulthood causes asymmetry in forelimb use. Plotting the percentage of total touches for each forepaw or both forepaws together, the *PTEN* deletion group had a slight, though insignificant increase in the percentage of right forepaw touches compared to controls. There was no significant difference in sidedness of spontaneous forepaw exploration for the *PTEN* deletion group compared to controls (two-way ANOVA, F(1, .004)= 0.0008059 p=0.9774 for *PTEN* deletion, F(2, 25)= 2.887 p= 0.0607 for paw sidedness, F(2, 22.9)= 2.628 p= 0.0775 for interaction) (Fig. 8B&C).

Mice with bilateral PTEN deletion exhibit improved motor learning 8 or more months post-deletion

Because mice with unilateral deletion of *PTEN* exhibited some impairment in rotarod, we wondered whether bilateral *PTEN* deletion would abrogate this impairment. To assess this, 10 PTEN/tdT mice and 9 tdT mice received bilateral AAV-Cre injections into the somatosensory cortex at 8 weeks of age and were tested on the rotarod every 2 months from 2 to 8 months post-injection (Fig. 8D–I).

At 2, 4, and 6 months following injection (when the mice were 4, 6, and 8 months old), mice with bilateral *PTEN* deletion performed comparably to controls over all 12 rotarod trials (Fig. 8E–I), see Figure legend for statistics). Surprisingly, at 8 months, mice with bilateral adult *PTEN* deletion demonstrated significantly better rotarod performance in comparison to controls, though differences at individual trials were not significant (Fig. 8H, two-way ANOVA, F(1, 101)= 4.181 p= 0.0422 for *PTEN* deletion, F(11, 891)= 3.357 p= 0.0003 for trial number, F(11, 142)= 0.5344 p= 0.8785 for interaction). Linear regression analysis revealed significantly improved motor learning in *PTEN* deletion mice (0.7012 RPM/trial for *PTEN* deletion versus 0.3113 RPM/trial for controls, F(1, 20)= 9.88212 p= 0.005113), though differences in baseline coordination were not significant (7.1 for *PTEN* deletion, 8.3 RPM for controls).

Based on the interim statistical analysis, we tested the mice again on the rotarod again at 10 months following injection); again, mice with *PTEN* deletion continued to demonstrate significantly better rotarod performance than controls (Fig. 8I, two-way ANOVA, F(1, 267)= 15.27 p< 0.0001 for *PTEN* status, F(11, 63)= 3.605 p<0.0001 for trial number, F(11, 53.5)= 0.2783 p= 0.9893 for interaction). Linear regression analysis showed that the slopes (rate of motor learning) of the *PTEN* deletion and control performance curves were not significantly different (for *PTEN* deletion slope= 0.5534 RPM/trial, control slope= 0.4162/trial, F(1, 20)= 2.63073 p= 0.1205), though baseline coordination was significantly improved in the *PTEN* deletion group (for *PTEN* deletion y-intercept= 7.705 RPM, control intercept= 6.430 RPM, F(1, 21)= 51.1406 p< 0.0001). Mice with bilateral *PTEN* deletion also attained higher average maximum speeds compared to controls. At 6 months post-injection, The highest average maximum attained speed for controls was 14.98 RPM vs. 16.63 RPM for *PTEN* deleted mice at 8 months post-deletion.

Testing in the cylinder task at 2, 4, 6, and 8 months post-deletion revealed no differences in forelimb use between mice with *PTEN* deletion vs. controls (Fig. 8J–M).

DISCUSSION

We show here that deleting *PTEN* in the sensorimotor cortex of adult mice leads to progressive growth of cell bodies, dendrites, and axons of cortical neurons that continues for at least 12 months post-deletion. Although there were increases in the number of primary dendrites and extent of dendritic branching, the basic pyramidal phenotype of cortical neurons was preserved (no ectopic apical dendrites, more basal than apical primary dendrites, and similar patterns of dendritic branching).

Progressive enlargement of CMN cell bodies with adult PTEN deletion

In our previous study of consequences of *PTEN* deletion at postnatal day 1 (Gutilla et al., 2016), cell bodies of CMNs were 1.7X larger than control CMNs at 12 months of age. We did not assess the time course of growth, however. Here we show that CMNs are about 1.5X larger than control CMNs at 12 months following *PTEN* deletion in early adulthood, and increase further to about 1.6X larger than control CMNs by 15 months. These results indicate that adult neurons can mount a continuous growth response, but the growth may be slower than what occurs with *PTEN* deletion during development. Interestingly, the largest percent increase occurs between 12–15 months post-deletion, suggesting that growth accelerates with increased time following deletion. This finding was unexpected, and further studies will be required to fully explore this late phase of growth.

In our previous study of mice with deletion of *PTEN* at P1, we also observed overall hypertrophy of the motor cortex and sometimes cortical expansion on the side of the *PTEN* deletion led to displacement of the superior sagittal fissue (Gutilla et al., 2016). With *PTEN* deletion in adult mice, we did not observe displacement of the superior sagittal fissue. There was focal cortical enlargement (a bump) in both PTEN/tdT and tdT mice, which was likely a response to surgical burr holes rather than *PTEN* deletion or AAV injections since control mice in our previous study did not have cortical enlargement following neonatal AAV injection.

Progressive increase in dendritic size and number following adult PTEN deletion

For technical reasons, quantitative analyses of dendritic parameters were done on pyramidal neurons in layers II–III. These actually provide an advantage over CMNs because the dendritic arbors of layer II/III pyramidal neurons are less elaborate than CMNs. Our results reveal increases in the number of primary dendrites extending from the soma (specifically basal primary dendrites), number of dendritic branch points, and number of intersections in concentric circle analysis from *PTEN* deleted pyramidal neurons. For most measures the *PTEN* deletion-induced morphological phenotype is more pronounced at 12 than 6 months following deletion. In contrast, comparison of control neurons from tdT mice at 6 vs. 12 months revealed decreases in dendritic arborization over time, consistent with age-related dendritic atrophy. Hence, in addition to inducing growth, *PTEN* deletion may prevent age-related dendritic atrophy.

One caveat is that the reconstructions don't capture the complete dendritic arbors. The 3D image stacks are oriented to capture the long axis of the pyramidal neuron, but dendrites extending laterally are captured only out to about 75–100μm, so distal branches are not visualized. In addition, distal apical dendritic arbors of most neurons were not captured within the area of the scan. Distal apical dendrites may be an additional site of structural modification following adult *PTEN* deletion, especially because of the known plasticity of these dendrites in the adult brain (Greenough et al., 1979).

One unanswered question is whether the new dendrites receive synaptic connections, and if so, whether synapse numbers are comparable to control neurons. We were not able to visualize spines in our 2-photon reconstructions, even at high resolution. A previous study of the consequences of shRNA-mediated knockdown of PTEN in dentate granule cells of adult mice revealed thicker dendrites and an overall increase in dendritic spines at 4 months post-injection (Luikart et al., 2011). A complication with interpreting these findings is that dentate granule cells are one of the few neuron types that exhibit adult neurogenesis, so the generalizability of the findings to other neuronal populations is unclear. An ideal way to address this question would be to identify newly-grown dendrites via sequential imaging in living animals and assess synapse number on newly-grown vs. previously existing dendrites.

PTEN deletion-induced increases in axon caliber without compensatory increases in myelination

Corticospinal tract axons emanating from *PTEN*-deleted CMNs were larger in diameter, without proportional increases in myelin, resulting in increased G-ratios. It is noteworthy that a recent study reported that selective promoter-driven deletion of *PTEN* in developing cerebellar granule cells led to enlargement of granule cell somata and increases in axon diameter that were accompanied by aberrant myelination of normally unmyelinated parallel fibers (Goebbels et al., 2017). The fact that myelin thickness did not increase in *PTEN*-negative CST axons may indicate that adjustments in myelin due to *PTEN* deletion-induced axon enlargement differ depending on whether the axon is normally myelinated, or on the developmental timing of the deletion. It remains to be seen whether changes in G-ratio in enlarged CST axons affect action potential propagation.

Persistent mTOR activation following PTEN deletion in adulthood

PTEN is a negative regulator of AKT/mTOR, so the expected result of *PTEN* deletion is persistent activation of mTOR. Strong evidence in support of this conclusion is the sustained activation of S6 phosphorylation in CMNs. Given mTOR's known role in promoting neuronal growth and dendritic outgrowth (Kumar et al., 2005; Urbanska et al., 2012), persistent mTOR activation due to *PTEN* deletion is a plausible mechanism for the growth that we describe here. The fact that growth can be initiated in mid-life supports the surprising conclusion that mature uninjured neurons retain the ability to reinitiate a robust growth response after they have reached their steady-state size. This finding supports the possibility of using *PTEN* modifying interventions to ameliorate neuronal atrophy following axon injury (Barron et al., 1988; Kobayashi et al., 1997; Schwab and Bartholdi, 1996).

Phosphorylation of ribosomal protein S6 is a downstream marker of mTOR activation, and may alter mRNA translation, but persistent activation of S6 phosphorylation is not likely to be the primary cause of neuronal growth. Activation of AKT and mTOR also leads to a host of other processes including signaling to the nucleus, which likely has multiple effects on gene expression. Understanding the mechanisms that actually contribute to growth is of great importance, especially in terms of potential clinical applications. The differential roles of the multiple processes triggered by persistent AKT/mTOR activation remain to be defined.

Functional consequences of adult PTEN deletion

Our initial analysis of functional consequences of *PTEN* deletion in the motor cortex revealed mixed effects on motor function as assessed by the rotarod and cylinder tasks. Mice with unilateral *PTEN* deletion exhibited slight rotarod impairment but maintained symmetry in spontaneous forelimb exploration. Mice with bilateral *PTEN* performed comparably to controls until 8 months post-deletion and exhibited improved rotarod performance to controls at later intervals.

Motor impairment with unilateral deletion involved impaired baseline performance that persisted over multiple trials (implying impaired coordination), lower maximum attained speed, but no difference in the rate of performance improvement (interpreted as motor learning). These performance trends are similar to that of mice one year following unilateral *PTEN* deletion during early postnatal development (Gutilla et al., 2016). A possible explanation for the impaired motor coordination and performance is that *PTEN* deletion is unilateral whereas the rotorod assesses overall motor function involving bilateral coordination.

Improved rotarod performance of mice with bilateral adult *PTEN* deletion manifested as improved baseline performance (motor coordination), a faster rate of performance improvement (motor learning), and higher maximum attained speeds. The fact that enhanced performance occurs in parallel with neuron growth invites the speculation that there is a causal relationship. In contrast to mice with *PTEN* deletion, control mice exhibited diminished rotarod performance at older ages. Again, diminished performance occurs in parallel with age-related decreases in dendrites suggesting a relationship. Our motor function analyses only assessed gross aspects of motor function following *PTEN* deletion in adult mice, and it will be of interest in future studies to test more sophisticated, fine motor functions. Unfortunately we did not assess motor function following bilateral *PTEN* deletion in neonatal mice, so we are unable to compare our present findings in the adult with the developing system.

PTEN deletion in non-neuronal cells

Expression of tdTomato following AAV-Cre transfection revealed tdT-positive cells with astrocyte morphology; these were confirmed to be astrocytes by co-immunolabeling with GFAP. Different AAV serotypes exhibit differential tropisms (Aschauer et al., 2013; Burger et al., 2004; Taymans et al., 2007), and the AAV-2 serotype used here has been shown to be relatively neuron-specific (Bartlett et al., 1998). Positive identification of tdT-positive

astrocytes highlights the utility of fluorescent reporter genes in identifying cell types that are transfected in low abundance. It remains to be seen whether *PTEN* deletion in non-neuronal cell types contributes to the anatomical and behavioral phenotypes reported here.

Implications of adult neuronal growth for neurodegenerative diseases and neurological injury

Neuronal and axonal atrophy are hallmarks of injury, many neurodegenerative diseases, and normal aging (Barron et al., 1989; Bronfman et al., 2000; Finch, 1993; McBride et al., 1989). Reducing such atrophy might be a promising way to attenuate the cognitive and functional declines associated with aging and neurodegenerative disease. Bringing together *PTEN*'s negative regulation of neuronal and axonal regeneration, neuronal survival, and neuronal growth, PTEN inhibition may be a promising way to abrogate injury and age-related atrophy as well as attenuate the negative pathophysiological consequences.

Acknowledgments

Thanks to Sara Jahangiri, Ilse Sears-Kraxberger, and Kelly Matsudaira Yee for superb technical assistance. Thanks to our funding sources, including the National Institutes of Health grant number NS047718 (to O.S.), 5T32GM008620 (to E.A.G.) and generous donations from Cure Medical, Research for Cure, Stonepole LTD, and Vinstar Development LTD.

Funding: This work was supported by the National Institutes of Health grant number NS047718 (to O.S.), 5T32GM008620 (to E.A.G.) and generous donations from Cure Medical, Research for Cure, Stonepole LTD, and Vinstar Development LTD.

References

Aschauer DF, Kreuz S, Rumpel S. Analysis of transduction efficiency, tropism and axonal transport of AAV serotypes 1, 2, 5, 6, 8 and 9 in the mouse brain. PloS one. 2013; 8:e76310. [PubMed: 24086725]

Barron KD, Banerjee M, Dentinger MP, Scheibly ME, Mankes R. Cytological and cytochemical (RNA) studies on rubral neurons after unilateral rubrospinal tractotomy: the impact of GM1 ganglioside administration. J Neurosci Res. 1989; 22:331–337. [PubMed: 2468791]

Barron KD, Dentinger MP, Popp AJ, Mankes R. Neurons of layer Vb of rat sensorimotor cortex atrophy but do not die after thoracic cord transection. J Neuropathol Exp Neurol. 1988; 47:62–74. [PubMed: 3275429]

Bartlett JS, Samulski RJ, McCown TJ. Selective and rapid uptake of adeno-associated virus type 2 in brain. Hum Gene Ther. 1998; 9:1181–1186. [PubMed: 9625257]

Bronfman FC, Moechars D, Van Leuven F. Acetylcholinesterase-positive fiber deafferentation and cell shrinkage in the septohippocampal pathway of aged amyloid precursor protein london mutant transgenic mice. Neurobiol Dis. 2000; 7:152–168. [PubMed: 10860782]

Burger C, Gorbatyuk OS, Velardo MJ, Peden CS, Williams P, Zolotukhin S, Reier PJ, Mandel RJ, Muzyczka N. Recombinant AAV viral vectors pseudotyped with viral capsids from serotypes 1, 2, and 5 display differential efficiency and cell tropism after delivery to different regions of the central nervous system. Mol Ther. 2004; 10:302–317. [PubMed: 15294177]

Danilov CA, Steward O. Conditional genetic deletion of PTEN after a spinal cord injury enhances regenerative growth of CST axons and motor function recovery in mice. Experimental neurology. 2015

Du K, Zheng S, Zhang Q, Li S, Gao X, Wang J, Jiang L, Liu K. Pten Deletion Promotes Regrowth of Corticospinal Tract Axons 1 Year after Spinal Cord Injury. The Journal of neuroscience : the official journal of the Society for Neuroscience. 2015; 35:9754–9763. [PubMed: 26134657]

Ferreira TA, Blackman AV, Oyrer J, Jayabal S, Chung AJ, Watt AJ, Sjostrom PJ, van Meyel DJ. Neuronal morphometry directly from bitmap images. Nature methods. 2014; 11:982–984. [PubMed: 25264773]

Finch CE. Neuron atrophy during aging: programmed or sporadic? Trends Neurosci. 1993; 16:104–110. [PubMed: 7681233]

Goebbels S, Wieser GL, Pieper A, Spitzer S, Weege B, Yan K, Edgar JM, Yagensky O, Wichert SP, Agarwal A, Karram K, Renier N, Tessier-Lavigne M, Rossner MJ, Karadottir RT, Nave KA. A neuronal PI(3,4,5)P3-dependent program of oligodendrocyte precursor recruitment and myelination. Nature neuroscience. 2017; 20:10–15. [PubMed: 27775720]

Greenough WT, Juraska JM, Volkmar FR. Maze training effects on dendritic branching in occipital cortex of adult rats. Behav Neural Biol. 1979; 26:287–297. [PubMed: 486026]

Gutilla EA, Buyukozturk MM, Steward O. Long-term consequences of conditional genetic deletion of PTEN in the sensorimotor cortex of neonatal mice. Experimental neurology. 2016; 279:27–39. [PubMed: 26896833]

Jaworski J, Sheng M. The growing role of mTOR in neuronal development and plasticity. Mol Neurobiol. 2006; 34:205–219. [PubMed: 17308353]

Kobayashi NR, Fan DP, Giehl KM, Bedard AM, Wiegand SJ, Tetzlaff W. BDNF and NT-4/5 prevent atrophy of rat rubrospinal neurons after cervical axotomy, stimulate GAP-43 and Talpha1-tubulin mRNA expression, and promote axonal regeneration. The Journal of neuroscience : the official journal of the Society for Neuroscience. 1997; 17:9583–9595. [PubMed: 9391013]

Kumar V, Zhang MX, Swank MW, Kunz J, Wu GY. Regulation of dendritic morphogenesis by Ras-PI3K-Akt-mTOR and Ras-MAPK signaling pathways. The Journal of neuroscience : the official journal of the Society for Neuroscience. 2005; 25:11288–11299. [PubMed: 16339024]

Kwon CH, Luikart BW, Powell CM, Zhou J, Matheny SA, Zhang W, Li Y, Baker SJ, Parada LF. Pten regulates neuronal arborization and social interaction in mice. Neuron. 2006; 50:377–388. [PubMed: 16675393]

Lewandowski G, Steward O. AAVshRNA-mediated suppression of PTEN in adult rats in combination with salmon fibrin administration enables regenerative growth of corticospinal axons and enhances recovery of voluntary motor function after cervical spinal cord injury. The Journal of neuroscience : the official journal of the Society for Neuroscience. 2014; 34:9951–9962. [PubMed: 25057197]

Liu K, Lu Y, Lee JK, Samara R, Willenberg R, Sears-Kraxberger I, Tedeschi A, Park KK, Jin D, Cai B, Xu B, Connolly L, Steward O, Zheng B, He Z. PTEN deletion enhances the regenerative ability of adult corticospinal neurons. Nature neuroscience. 2010; 13:1075–1081. [PubMed: 20694004]

Luikart BW, Schnell E, Washburn EK, Bensen AL, Tovar KR, Westbrook GL. Pten knockdown in vivo increases excitatory drive onto dentate granule cells. The Journal of neuroscience : the official journal of the Society for Neuroscience. 2011; 31:4345–4354. [PubMed: 21411674]

McBride RL, Feringa ER, Garver MK, Williams JK Jr. Prelabeled red nucleus and sensorimotor cortex neurons of the rat survive 10 and 20 weeks after spinal cord transection. J Neuropathol Exp Neurol. 1989; 48:568–576. [PubMed: 2769309]

Park KK, Liu K, Hu Y, Smith PD, Wang C, Cai B, Xu B, Connolly L, Kramvis I, Sahin M, He Z. Promoting axon regeneration in the adult CNS by modulation of the PTEN/mTOR pathway. Science. 2008; 322:963–966. [PubMed: 18988856]

Rothwell PE, Fuccillo MV, Maxeiner S, Hayton SJ, Gokce O, Lim BK, Fowler SC, Malenka RC, Sudhof TC. Autism-associated neuroligin-3 mutations commonly impair striatal circuits to boost repetitive behaviors. Cell. 2014; 158:198–212. [PubMed: 24995986]

Schwab ME, Bartholdi D. Degeneration and regeneration of axons in the lesioned spinal cord. Physiological reviews. 1996; 76:319–370. [PubMed: 8618960]

Sperow M, Berry RB, Bayazitov IT, Zhu G, Baker SJ, Zakharenko SS. Phosphatase and tensin homologue (PTEN) regulates synaptic plasticity independently of its effect on neuronal morphology and migration. The Journal of physiology. 2012; 590:777–792. [PubMed: 22147265]

Takeuchi K, Gertner MJ, Zhou J, Parada LF, Bennett MV, Zukin RS. Dysregulation of synaptic plasticity precedes appearance of morphological defects in a Pten conditional knockout mouse

model of autism. Proceedings of the National Academy of Sciences of the United States of America. 2013; 110:4738–4743. [PubMed: 23487788]

Taymans JM, Vandenberghe LH, Haute CV, Thiry I, Deroose CM, Mortelmans L, Wilson JM, Debyser Z, Baekelandt V. Comparative analysis of adeno-associated viral vector serotypes 1, 2, 5, 7, and 8 in mouse brain. Hum Gene Ther. 2007; 18:195–206. [PubMed: 17343566]

Urbanska M, Gozdz A, Swiech LJ, Jaworski J. Mammalian target of rapamycin complex 1 (mTORC1) and 2 (mTORC2) control the dendritic arbor morphology of hippocampal neurons. The Journal of biological chemistry. 2012; 287:30240–30256. [PubMed: 22810227]

Williams MR, DeSpenza T Jr, Li M, Gulledge AT, Luikart BW. Hyperactivity of newborn Pten knock-out neurons results from increased excitatory synaptic drive. The Journal of neuroscience : the official journal of the Society for Neuroscience. 2015; 35:943–959. [PubMed: 25609613]

Zukor K, Belin S, Wang C, Keelan N, Wang X, He Z. Short hairpin RNA against PTEN enhances regenerative growth of corticospinal tract axons after spinal cord injury. The Journal of neuroscience : the official journal of the Society for Neuroscience. 2013; 33:15350–15361. [PubMed: 24068802]

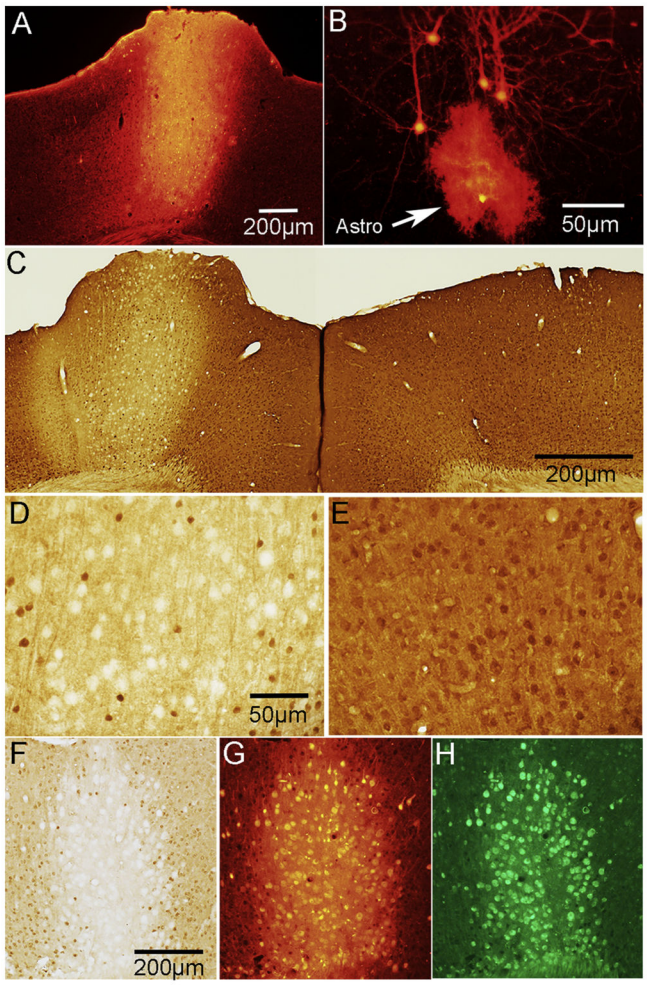

Figure 1.

Expression of tdTomato and concurrent *PTEN* deletion in PTEN/tdT mice following AAV-Cre injection in adult mice. **A.** tdTomato expression in the area of AAV-Cre injection into the left sensorimotor cortex. **B.** tdT-labeled pyramidal neurons and one astrocyte in the penumbra of the injection (arrowhead indicates astrocyte). **C.** PTEN immunostain of left and right motor cortex; area of deletion (about 1mm diameter) corresponds to the area of tdT expression in panel A. **D.** Higher magnification of layer V in the area of PTEN deletion; note PTEN-negative “ghost cells”. **E.** Layer V in the homotypic region of the contralateral cortex in the same section as D. **F.** High magnification of ghost cells with bright field microscopy; **G.** Same field in phase contrast. Arrowheads indicate ghost cells.

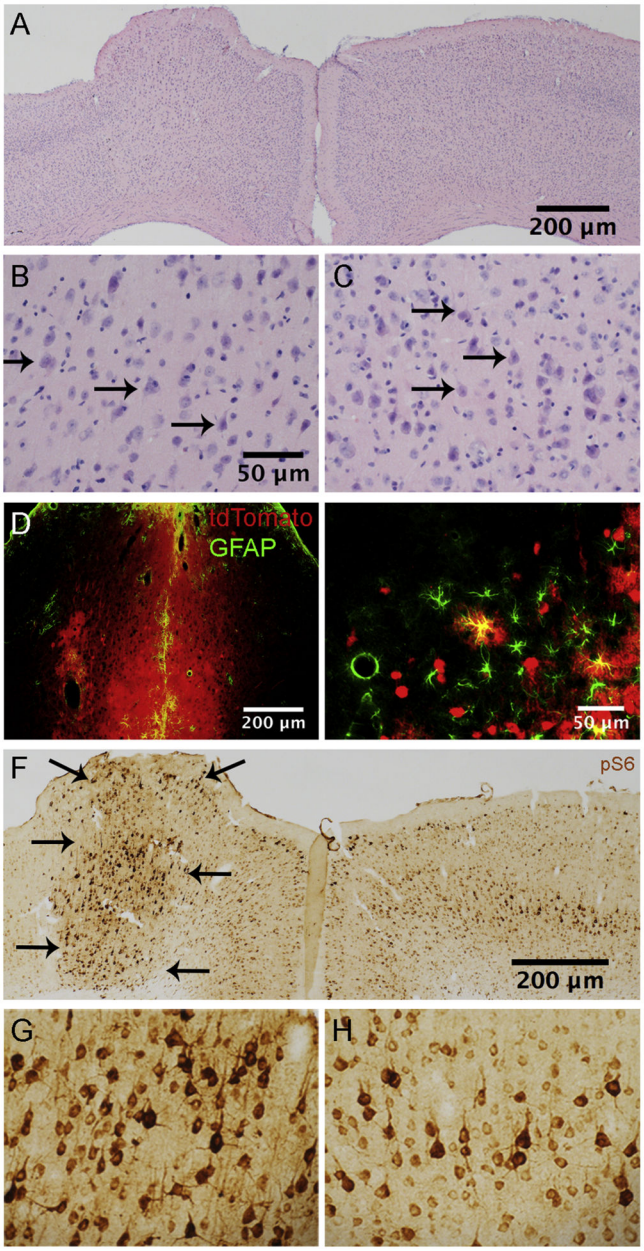

Figure 2.

Histology following *PTEN* deletion in adult mice. **A.** H&E stained section illustrating cortical architecture ipsi and contralateral to the AAV-Cre injection at 12 months post-AAV. Arrows indicate the area of the injection. **B.** High magnification view of layer V in the area of *PTEN* deletion from the section in A. **C.** Layer V of the contralateral cortex from the section in A. **D.** Section at the site of needle track from the intracortical injection immunostained for GFAP. **E.** Nearby area outside the core of the injection from the section in D. Note that some astrocytes are co-labeled for GFAP and tdT (arrowheads). **F.** Immunostaining for pS6 (antibody against p-Ser 235/236) in the area of deletion and contralateral cortex (same mouse shown in panel A). Note distinct boundary (arrows)

between area with elevated pS6 immunostaining and surrounding regions **G.** Higher magnification view of pS6-positive neurons in the region of *PTEN* deletion shown in F. **H.** pS6 immunostaining in the homologous region of the contralateral control motor cortex.

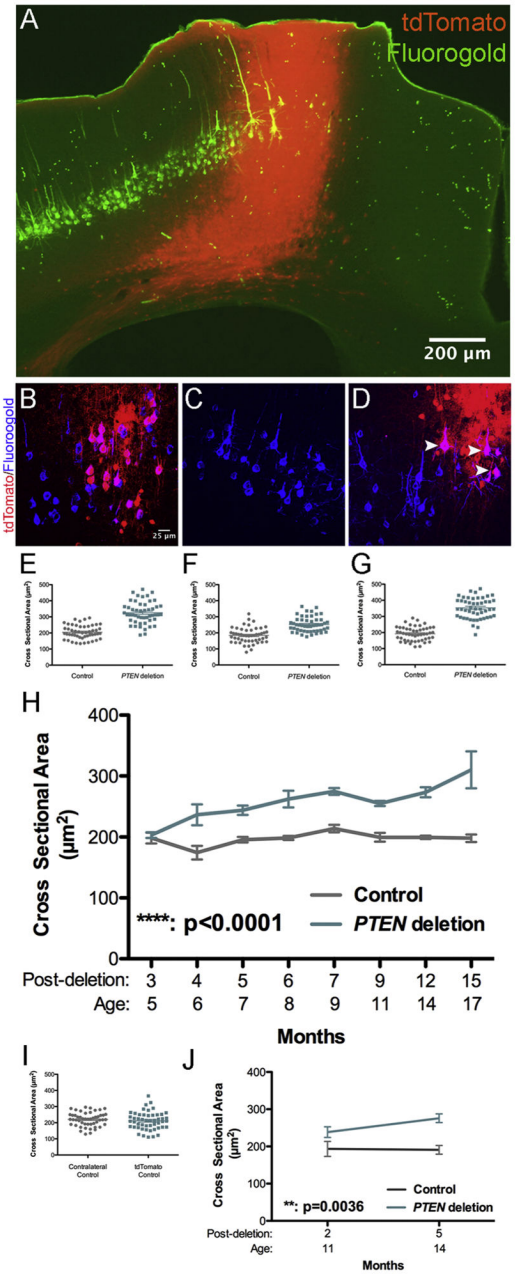

Figure 3.

Age-dependent neuronal growth following *PTEN* deletion in adulthood. **A.** Section from a PTEN/tdT mouse that had received Fluorogold into the cervical spinal cord; section is immunostained for FG and tdT is visualized by native fluorescence. Two images of the same field were taken with NB and NG illumination on an Olympus AX80 microscope. Paired images were converted to 8-bit, imported into ImageJ and FG fluorescence in NB was assigned to the green channel and tdT fluorescence in NG was assigned to the red channel. **B.** 2D projection of a 3D reconstruction illustrating cortical motoneurons (CMNs) from a tdT mouse, 4 months following AAV-Cre injection retrogradely labeled with FG (blue) some of which express tdT (red). Co-labeled cells are magenta (white arrowheads). **C.** 2D

projection of a 3D multiphoton reconstruction from the homologous area of the motor cortex contralateral to the area shown in A; note all CMNs are labeled by Fluorogold only. **D.** 2D projection of a 3D reconstruction illustrating CMNs retrogradely labeled by Fluorogold and tdTomato from a PTEN/tdT mouse (arrowheads). **E.–G.** Scatter plots of CMN cell body sizes from 3 PTEN/tdT mice 15 months following *PTEN* deletion. **H.** Average cell body size of *PTEN* deleted and control CMNs at different times post AAV-Cre injection. Sidak's post-test of differences at particular time points: 3 months: NSD ($p>0.9999$). 4 months: $p=0.0006$. 5 months: $p=0.0181$, 6 months: $p=0.0023$, 7 months: $p=0.0445$, 9 months: $p=0.0308$, 12 months: $p=0.0008$, 15 months, $p<0.0001$). **I.** Scatter plot of cell size from a control tdT mouse, 12 months after AAV-Cre injection. **J.** Average cell body size of *PTEN* deleted and control CMNs after *PTEN* deletion at 9 months of age.

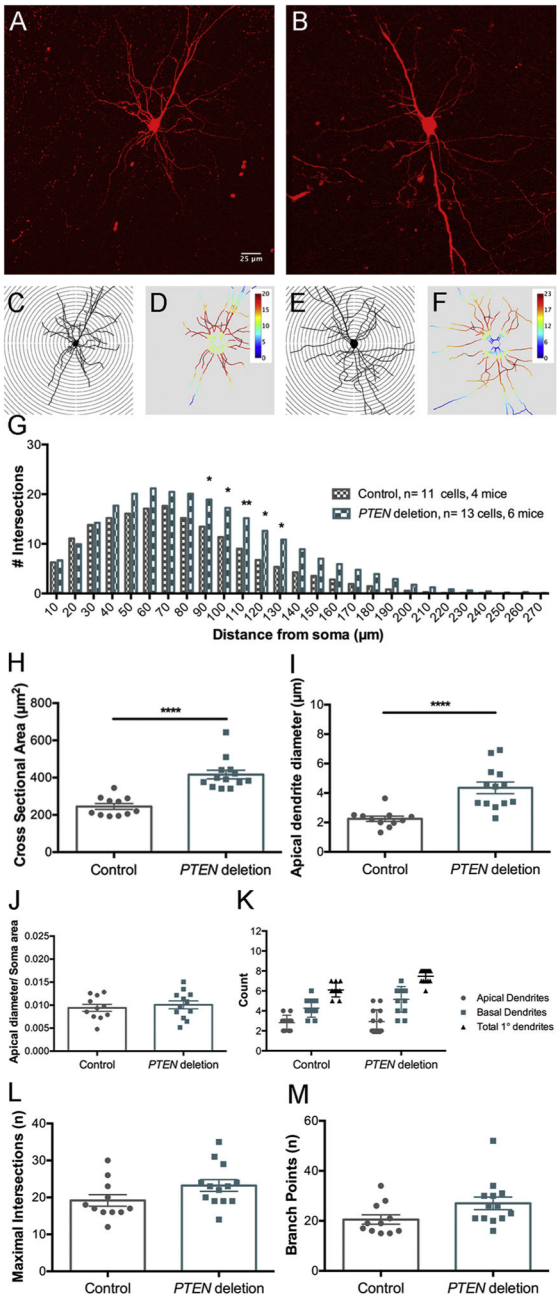

Figure 4.

Sholl analysis of dendritic number and arborization of cortical pyramidal neurons 6 months following *PTEN* deletion. **A.** Flattened projection of a 3D reconstruction of tdTomato-labeled control pyramidal neuron from a cleared thick section. **B.** Flattened projection of a tdTomato-labeled *PTEN* deleted pyramidal neuron. **C.** Traced projection of neuron in A overlaid with concentric circles for Sholl analysis. **D.** Heat map of C generated by ImageJ Sholl Analysis Program, warmer colors represent a greater number of dendritic intersections, cooler colors represent fewer dendritic intersections. **E.** Traced projection of B. overlaid with concentric circles. **F.** Heat map of E generated by Sholl Analysis Program. **G.** Average

Sholl concentric circle analysis data from 11 control and 13 *PTEN* deleted pyramidal neurons. Asterisks indicate distances at which differences were significant at $p<.05$ by Sidak's post-test (for 90μm p=0.0281, 100μm p=0.0118, 110μm p=0.0062, 120 μm p=0.0113, 130μm p=0.0273). **H.** Cross-sectional area of soma of *PTEN* deleted pyramidal neurons vs. controls. **I.** Diameter of the large apical dendrite (30 μm away from the center of the soma). **J.** Ratio of the diameter of the apical dendrite to the cross-sectional area of the soma. **K.** Number of basal and apical primary dendrites in *PTEN* deleted pyramidal neurons vs. controls. **L.** Maximal number of intersections at any distance from the soma (concentric circle with highest number of crossings). **M.** Total number of branch points in *PTEN* deleted vs. control neurons.

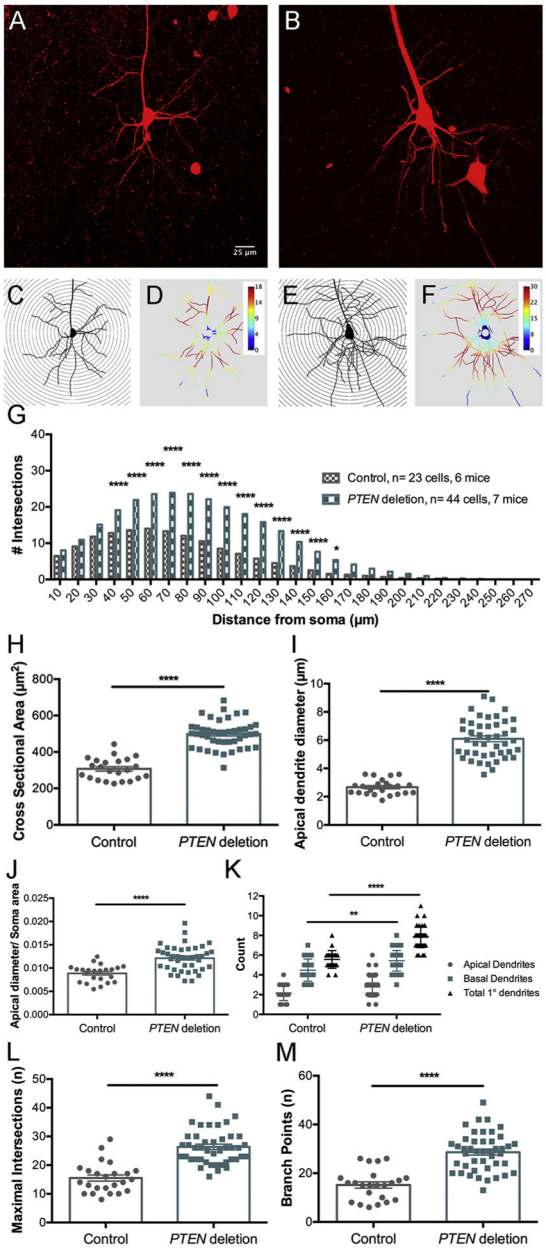

Figure 5.

Sholl analysis of dendritic number and arborization 12 months following *PTEN* deletion. **A.** Flattened projection of a 3D reconstruction of tdTomato-labeled control neuron from a cleared thick section. **B.** Flattened projection of a tdTomato-labeled *PTEN* deleted neuron. **C.** Traced projection of A. overlaid with concentric circles for Sholl analysis. **D.** Heat map of C generated by Sholl Program. **E.** Traced projection of B overlaid with concentric circles. **F.** Heat map of E generated by Sholl Program. **G.** Average intersections for the Sholl concentric circle analysis data from 23 control and 44 *PTEN* deleted pyramidal neurons. Asterisks indicate distances at which differences were significant at $p<.05$ by Sidak's post-test (for 40µm–150µm $p<0.0001$, 160µm $p=0.0102$). **H.** Cross-sectional area of soma. **I.**

Diameter of the large apical dendrite (30 μm away from the center of the soma). **J.** Ratio of dendrite diameter to cross-sectional area of the soma. **K.** Number of basal and apical primary dendrites. **L.** Maximal number of intersections at any distance from the soma (concentric circle with highest number of crossings). **M.** total number of branch points in *PTEN* deleted vs. control neurons.

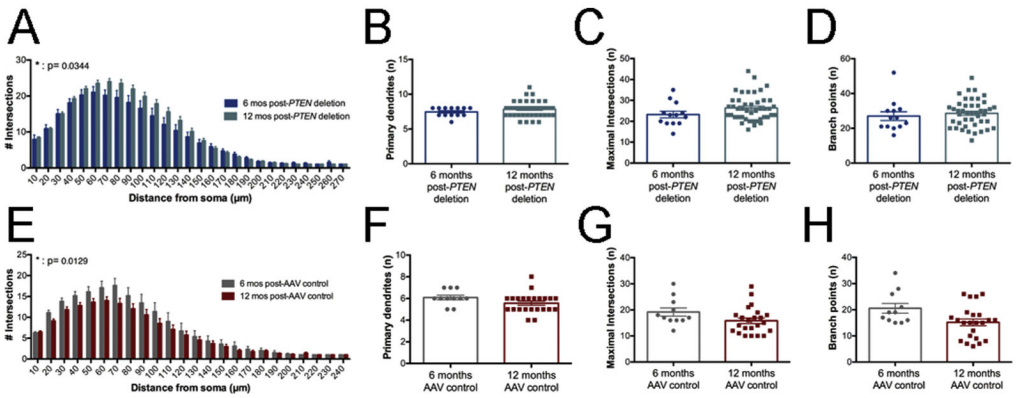

Figure 6.

PTEN deleted neurons exhibit age-related gains in dendritic arborization; control neurons exhibit age-related losses. **A.** Age-based comparisons of Sholl data from *PTEN* deletion pyramidal neurons at 6 vs. 12 months post-deletion. **B.** Number of primary dendrites of *PTEN*-deleted neurons at 6 vs. 12 months post-injection (8 and 14 months of age). **C.** Maximal intersections of *PTEN* deleted neurons at 6 vs. 12 months post-deletion. **D.** Number of branch points in *PTEN* deleted neurons at 6 vs. 12 months post-deletion. **E.** Age-based comparisons of Sholl data from control pyramidal neurons at 6 vs.12 months post-AAV injection. **F.** Number of primary dendrites of control neurons at 6 vs. 12 months post-injection. **G.** Maximal intersections at 6 vs.12 months post-injection. **H.** Number of branch points at 6 vs. 12 months post-injection.

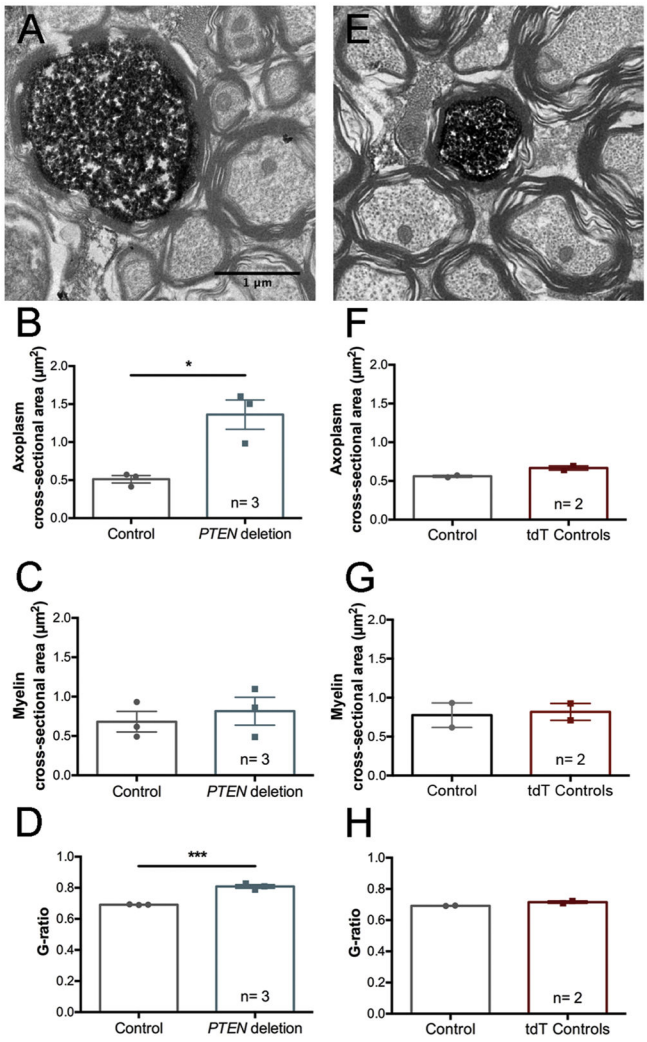

Figure 7.

Increases in CST axon diameter and decreases in G-ratio following adult *PTEN* deletion. **A.** Electron microscopic images of tdT-positive (*PTEN* deleted) and nearby unlabeled CST axons from PTEN/tdT mice 12 months post-AAV-Cre. **B.** Points in bar graphs are the average cross-sectional area of the axoplasm of *PTEN* deleted vs. nearby unlabeled control axons in each mouse. **C.** Points in bar graphs are the average cross-sectional area of the myelin sheath of *PTEN* deleted vs. nearby unlabeled control axons in each mouse. **D.** Points in bar graphs are the average G-ratio for *PTEN* deleted vs. nearby unlabeled control axons in each mouse. **E.** tdTomato-positive brainstem axons in tdT control mice one year following AAV-Cre injection. **F, G &H.** Graphs are for the same values as B, C &D for tdT control mice (two-way ANOVA, for control type $F(1, 6)= 2.040$ $p= 0.2031$, for structure measured $F(2, 6)= 32$ $p= 0.0006$, for interaction $F(2, 6)= 0.3980$ $p= 0.6881$, Sidak's post-test for axoplasm area: $p> 0.9999$, for myelin area: $p> 0.9999$). G-ratio: (student's t-test, $p= 0.0840$).

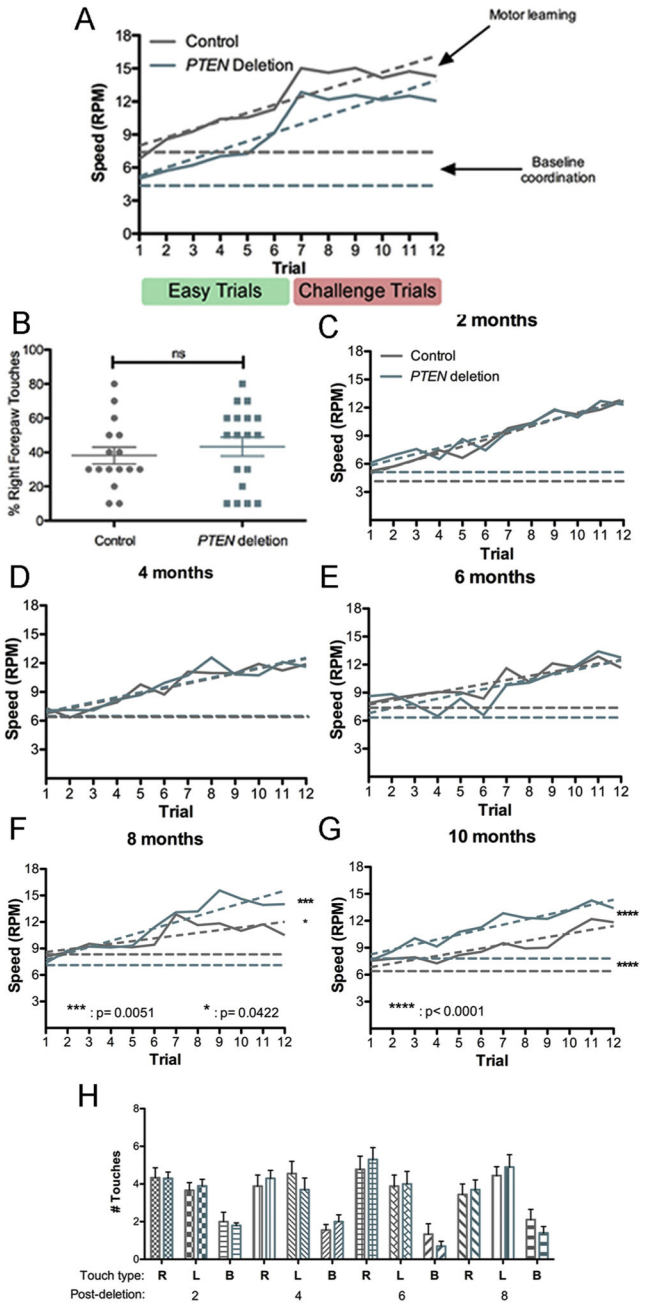

Figure 8.

Motor learning and forelimb exploration following adult unilateral or bilateral *PTEN* deletion. **A.** Plot of rotarod performance (maximal speed attained) over trials of mice with unilateral *PTEN* deletion vs. controls. Easier trials 1–6: starting speed of the rod was 4 rotations per minute (RPM) and the acceleration 0.1 RPM/second (RPM/s). Challenge trials 7–12: starting speed of the rod was increased to 6 RPM with an acceleration of 0.2 RPM/s. **B.** Percent right forepaw touches by mice with unilateral *PTEN* deletion in the left motor cortex in comparison to controls. **C.** Plot of rotarod performance (maximal speed attained) over trials of mice with bilateral PTEN deletion vs. controls at 2 months post-AAV. **D.**

Rotarod performance at 4 months post-AAV. **E.** Rotarod performance at 6 months post-AAV. **F.** Rotarod performance at 8 months post-AAV injection. **G.** Rotarod performance at 10 months post-AAV. **H.** Assessment of spontaneous forelimb exploration in the cylinder task at 2–8 months post-injection. Two-way ANOVA revealed no significant differences at any time point.

Table 1

Mice used for cell body size measurements and unilateral behavior assessment.

Months Post AAV-Cre	# PTEN/tdT mice	# tdT mice	# Injected with Fluorogold	# Used in behavior at 6 months post-deletion
3	n=6	n=2	n=8	n=0
4	n=5	n=0	n=5	n=0
5	n=5	n=0	n=5	n=0
6	n=3	n=2	n=5	n=0
7	n=4	n=0	n=4	n=4 PTEN/tdT
8	n=3	n=0	n=3	n=3 PTEN/tdT
9	n=6	n=0	n=8	n=4 PTEN/tdT
12	n=5	n=2	n=6	n=4 PTEN/tdT
15	n=3	n=2	n=5	n=3 PTEN/tdT

Table 2

Summary of mice used for Sholl analysis.

Mouse	Time point	Age	Group	Genotype	Sex	# of cells	Total cells
1	6 months	8 months	*PTEN* deletion	PTEN/tdT	M	1	
2	6 months	8 months	*PTEN* deletion	PTEN/tdT	M	5	
3	6 months	8 months	*PTEN* deletion	PTEN/tdT	M	1	
4	6 months	8 months	*PTEN* deletion	PTEN/tdT	F	3	
5	6 months	8 months	*PTEN* deletion	PTEN/tdT	F	1	
6	6 months	8 months	*PTEN* deletion	PTEN/tdT	F	1	n= 12
1	6 months	8 months	Control	tdT	M	4	
2	6 months	8 months	Control	tdT	F	1	
3	6 months	8 months	Control	tdT	F	3	
4	6 months	8 months	Control	tdT	F	3	n= 11
1	12 months	14 months	*PTEN* deletion	PTEN/tdT	M	7	
2	12 months	14 months	*PTEN* deletion	PTEN/tdT	M	5	
3	12 months	14 months	*PTEN* deletion	PTEN/tdT	M	4	
4	12 months	14 months	*PTEN* deletion	PTEN/tdT	F	4	
5	12 months	14 months	*PTEN* deletion	PTEN/tdT	F	4	
6	12 months	14 months	*PTEN* deletion	PTEN/tdT	F	6	
7	12 months	14 months	*PTEN* deletion	PTEN/tdT	F	11	n= 41
1	12 months	14 months	Control	tdT	F	1	
2	12 months	14 months	Control	tdT	F	6	
3	12 months	14 months	Control	tdT	F	2	
4	12 months	14 months	Control	tdT	F	4	
5	12 months	14 months	Control	tdT	M	5	
6	12 months	14 months	Control	tdT	M	5	n= 23